12-17-2014

Aligning Carbon Fibers in Micro-Extruded Composite Ink

Chaitanya G. Mahajan

ROCHESTER INSTITUTE OF TECHNOLOGY

ALIGNING CARBON FIBERS IN MICRO-EXTRUDED COMPOSITE INK

Chaitanya G. Mahajan

Thesis submitted to the Faculty of the

Rochester Institute of Technology

In partial fulfillment of the requirements for the degree of

Master of Science in Industrial Engineering

Thesis Committee:

Dr. Denis Cormier

Dr. Marcos Esterman

Department of Industrial and Systems Engineering

December 17, 2014

DEPARTMENT OF INDUSTRIAL AND SYSTEMS ENGINEERING

KATE GLEASON COLLEGE OF ENGINEERING

ROCHESTER INSTITUTE OF TECHNOLOGY

ROCHESTER, NEW YORK

CERTIFICATE OF APPROVAL

December 17, 2014

M.S. DEGREE THESIS

The M.S. Degree Thesis of Chaitanya Mahajan

has been examined and approved by the

thesis committee as satisfactory for the

thesis requirement for the

Master of Science degree

Approved by:

Dr. Denis Cormier, Thesis Advisor

Dr. Marcos Esterman, Committee Member

Abstract

Direct write processes include a wide range of additive manufacturing techniques with the ability to fabricate structures directly onto planar and non-planar surfaces. Most additive manufacturing techniques use unreinforced polymers to produce parts. By adding carbon fiber as a reinforcing material, properties such as mechanical strength, electrical conductivity, and thermal conductivity can be enhanced. Carbon fibers can be long and continuous, or short and discontinuous. The strength of carbon fiber composite parts is greatly increased when the fibers are preferentially aligned. This research focuses on increasing the strength of additively manufactured parts reinforced using discontinuous carbon fibers that have been aligned during the micro extrusion process.

A design of experiments (DOE) approach was used to identify significant process parameters affecting fiber alignment. Factors such as the length of carbon fibers, nozzle diameter, fiber loading fraction, air pressure, translational speed and standoff distance were considered. A two dimensional Fast Fourier Transform (2D FFT) was used to quantify the degree of fiber alignment in the extruded composite inks. ImageJ software supported by an oval profile plugin was used with micrographs of printed samples to obtain the carbon fiber alignment values. The optimal value for the factors was derived by identifying the significant main and interaction effects.

Based on the results of the DOE, tensile test samples were printed with fibers aligned parallel and perpendicular to the tensile axis. A standard test method for tensile properties of plastic revealed that the extruded parts with fibers aligned along the tensile axis were better in tensile strength and modulus.

Acknowledgements

I wish to express my most sincere gratitude to my advisor Dr. Denis Cormier for giving me the opportunity to work on this research and for his continuous support, motivation and guidance. I feel fortunate to learn from his breadth of knowledge and valuable research literature in the field of additive manufacturing. I would also like to thank Dr. Marcos Esterman for his insights and guidance during the course of my thesis.

Additionally, I would like to thank John Bonzo and Michael Buffalin for their kind help and suggestions. Their experience in fabricating parts with different machines was of great help for my thesis. Sincere thanks to the entire faculty in the Industrial & Systems Engineering department for their help and support as always.

I would like to extend my gratitude to my fellow Industrial engineering graduate students, roommates and to all who helped me throughout my master's journey. A special thanks to Prachi for being with me through thick and thin.

Finally, I want to thank my parents and sister for their love and support, their spiritual point of view in life has helped me get through tough times with ease.

Table of Contents

List of Figures

List of Tables

Chapter 1: Introduction

1.1 Carbon Fiber Composites and Their Advantages

A composite material can be defined as a combination of two or more materials that result in better properties than those of the individual components used alone (Campbell, 2010). A composite with at least one of the fillers consisting of carbon fibers and matrix as either a polymer, metal or ceramic is referred to as a carbon fiber composite. Some of the advantages of carbon fiber composites include weight reduction, high strength, corrosion resistance, and chemical resistance. Carbon fibers are used to increase electrical and thermal conductivity of the composite. Moreover, carbon fibers have a very low coefficient of thermal expansion, hence they are often added to lower the thermal expansion of a material during processing (Chung, 1994). Various industries such as aerospace, medical, and automotive are replacing many metal components with polymer matrix carbon fiber composites.

1.2 Geometric Limitations of Fiber Composites

In a composite material, the reinforcing phase is of primary importance in the strengthening of the composite. There is a practical limit of about 70 volume percent reinforcement that can be added to form a composite (Campbell, 2010). In a chopped carbon fiber composite, as the carbon fiber content increases, the fiber interactions also increase to produce a dense mesh. This is because there is too little matrix to support the fibers effectively. Lee *et al.* (2007) observed that as the weight percentage of chopped carbon fibers increase beyond a point, the fiber orientation becomes more random, and debonding area becomes wider causing the tensile strength to decrease.

1.3 Fiber Composite Manufacturing Processes

Reinforcing fibers in composite materials can be in the form of long continuous fibers, discontinuous fibers, or particles. Continuous fibers have long aspect ratios and have a preferred orientation, while discontinuous fibers have short aspect ratios and generally have a random orientation. Due to the fiber orientation, the strength and stiffness of continuous fiber composites are much greater than those of discontinuously reinforced fiber composites. Continuous fiber composites are often made into laminates by stacking single sheets of continuous fibers in different orientations to obtain desired strength and stiffness properties. Short fiber composites are generally made using injection or compression molding. Figure 1 shows the various fabrication processes used to produce polymer matrix composites. In recent years, fiber reinforced composites have also been manufactured using three dimensional printing.

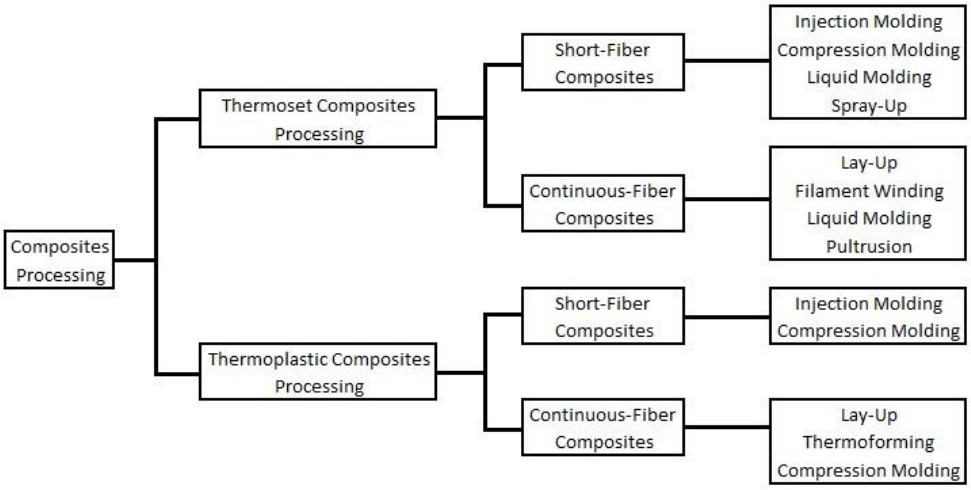

Figure 1: Composite fabrication processes (Adapted from (Campbell, 2010))

1.4 Three Dimensional (3D) Composite Printing

3D Printing is a manufacturing process that can be used to produce complex geometries with a large variety of materials. It repeatedly prints layers of finite thickness from a 3D Computer Aided Design (CAD) model to build a part one layer at a time. In addition to printing geometrically complex parts, other advantages of 3D printing include the ability to reduce the weight of a part, and reduced material waste.

Until very recently, 3D printed polymer components have been made from unreinforced thermoplastics or Ultraviolet (UV) curable photopolymers. While very impressive results have been obtained in some cases, the mechanical properties of these polymers have not come close to those achieved by reinforced polymer matrix composites. A very recent development has been the 3D printing of reinforced thermoplastics with increased strength and stiffness. The Mark One printer from MARKFORG3D (markforged.com) prints parts using carbon fiber, fiberglass, or Kevlar fibers in a nylon filament. It uses continuous fiber reinforcement, rather than chopped fibers, in a thermoplastic resin to print parts. As of this writing, the Mark One printer is not yet commercially available. No published and verified mechanical properties are yet available for this system.

To determine the fiber loading and the degree of fiber alignment, Compton & Lewis (2014) used a micro extrusion process to align discontinuous carbon fibers in an epoxy based ink. A significant increase in Young's modulus from 8.06±0.45 *GPa* for transverse print direction to 24.5±0.83 *Gpa* for longitudinal print direction was observed. Failure strength values also increased from 43.9±4.1 *Mpa* for transverse print direction to 66.2±6.1 *Mpa* for longitudinal print direction.

So far, 3D printing has been developed for thermoplastic and photopolymers, but very few options exist for use with epoxy resins. Discontinuous carbon fibers can be used with epoxy resin to increase strength if the fibers are aligned with the direction of the applied force.

1.5 Thesis Objective

Processes for making continuously reinforced carbon fiber composites tend to be quite labor intensive. Discontinuous fiber composites are therefore typically used where cost is the main factor, and where strength and stiffness are less important. However, the strength of discontinuously reinforced fiber composites can approach those of continuous fiber composites if their aspect ratio is sufficient and the fibers are aligned. In practice however, it is difficult to align discontinuous fibers (Campbell, 2010). The objective of this thesis is to find the most significant factors that influence fiber alignment in micro extruded carbon epoxy inks. The second objective is to use the results to determine the effect of the aligned fibers on tensile strength. Various fiber alignment processes and their effect on mechanical properties are detailed in Chapter 2.

Chapter 2: Literature Review

Various mathematical models exist which predict tensile strength based on fiber length and fiber orientation distribution. Fu & Lauke (1996) provide mathematical models that predict the tensile strength of short fiber composites based on both fiber length distribution and fiber orientation distribution. They observed that the strength of the composite increases with increase in fiber orientation coefficient. Kuriger, Alam, & Anderson (2001) theoretically and experimentally demonstrated that the composite strength increases as the degree of fiber alignment and fiber length increase. Figure 2 illustrates the effect of fiber orientation on tensile strength of a fiber reinforced polyester composite (Bagherpour, 2012).

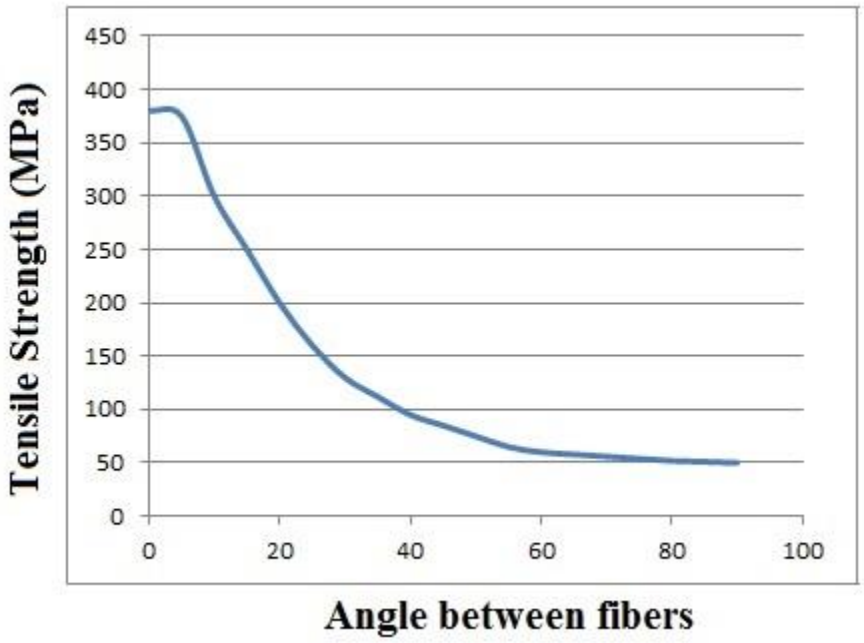

Figure 2: Effect of fiber orientation on tensile strength of FRP composite (Adapted from (Bagherpour, 2012))

Figure 2 indicates that the tensile strength is highest when the fibers are aligned with the tensile axis. Various processes which allow fibers to be aligned in a composite are described as follows.

2.1 Injection Molded Polymer Matrix Composites

Injection molding is widely used to produce products with intricate net shapes. Lightweight parts with good mechanical properties can be injection molded using fiber-reinforced polymeric composites. Dimensional accuracy, mechanical properties, and micro structure of the final product are greatly influenced by anisotropy caused by the fiber orientation generated by the flow during injection molding (S. Lee, Yang, Ko, & Youn, 1997). The fiber orientation of Short Fiber-Reinforced Thermoplastics (SFRTP) is observed under conditions of converging, diverging, and shearing flows. All these three types of flows have different effects on fiber orientations; the convergent flow at die entrance results in high fiber alignment, diverging flow causes fibers to align normal to the major flow direction, whereas the shear flow has the effect of disorienting the aligned fibers caused by convergent flow (Crowson, Folkes, & Bright, 1980).

Fiber orientation is also observed in the filling and packing stages of the injection molding process. The fiber orientation is mainly determined during the filling stage, with additional slight changes taking place during the packing stage (Matsuoka, Takabatake, Inoue, & Takahashi, 1990). Fibers tend to get more transverse orientation along the centerline of the stretching flow in the mid plane during the packing stage (Shokri & Bhatnagar, 2012).

2.2 Aligning Fibers Using Electric Fields

2.2.1 Dielectrophoresis

Dielectrophoresis is the motion of particles in a fluid induced by a non-uniform electric field upon a neutral object (Pohl & Crane, 1971). Pohl *et al.* (1971) described electrophoresis as the resulting particle motion caused by electrostatic interaction between charged particles and the field. It involves the application of direct current or low frequency electric field which is usually homogeneous. Dielectrophoresis is the transitional motion of the neutral particle due to interaction of a non-uniform electric field with all of its dipoles. It involves alternating current with a wide range of frequencies and

inhomogeneous electric field (Pethig & Markx, 1997). Figure 3 shows the basic principle of dielctrophoresis.

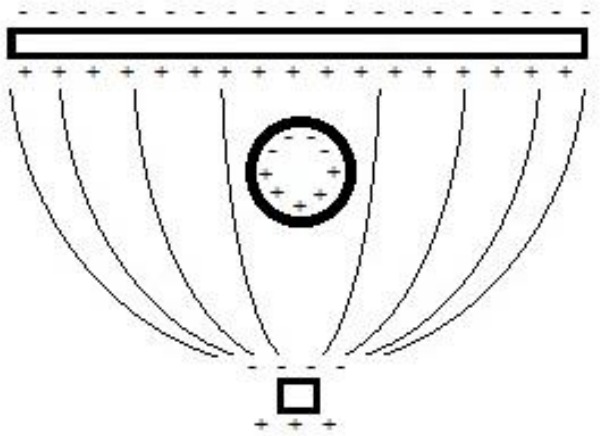

Figure 3: Polarization of a neutral body in a non-uniform electric field (Adapted from (Hughes, 2000))

A neutral charged particle becomes polarized in the presence of an electric field. Due to the non-uniformity of the electric field, the particle drifts towards the stronger part of the electric field. Dielctrophoersis has been used to align fibers during curing of the resin. Van den Ende *et al.* (2012) fabricated PZT short fiber polymer composite material using dielectrophoresis, where the PZT fibers became aligned parallel with the direction of the electric field.

2.2.2 Field-Aided Microtailoring (FAiMTa) Technology

Kim & Shkel (2004) developed a process which uses electric fields to locally modify the distribution and orientation of inclusions in a polymer. They refer to their technique as Field-Aided Microtailoring (FAiMTa). Either an Alternating Current (AC) or Direct Current (DC) field can be used to orient the organic or inorganic particles. The electric field can be applied to produce composites with uniform oriented structure or locally modified surfaces in selected areas.

G. Kim, Moeller, & Shkel (2004) studied the rotation of glass fibers in an AC electric field having a frequency $f = 5Hz$ and magnitude $E = 0.7\ kV/mm$. The study demonstrated the use of FAiMTa technology

to modify composites consisting of ceramic, graphite or glass fiber inclusions in epoxy. The polymeric composites can be microtailored regardless of the conductivity of the fillers.

2.3 Freeform Fabrication of Fiber Reinforced Composites

Freeform fabrication is a process whereby three dimensional parts are built by writing successive layers of material on a substrate. As an example, Calvert, Lin, & Martin (1997) describe a process by which ink consisting of chopped fibers blended in epoxy resin is written onto a heated substrate to initiate curing. Hydrophobic fumed silica is added to allow a flat layer to be written and initiates slow curing which allows each layer to support those deposited on top of it. The study's authors discuss the influence of short carbon fiber content and its length on the modulus of the composite. The study showed the following results:

- As the fiber content increases, the modulus of the composite also increases.
- As the fiber length increases while maintaining constant fiber volume fraction, the modulus of the composite increases.

Peng, Lin, & Calvert (1999) extruded glass fiber reinforced epoxy resin and observed the orientation of glass fibers with different process parameters such as write head speed and diameter of syringe needle. The study concluded the following:

- As the write head speed increases with the same needle size and fluid flow rate, the fiber distribution shifts to higher orientation.
- At constant flow rate and head speed, changing the diameter of the needle showed no significant change on fiber orientation.

Compton and Lewis (2014) created epoxy based inks with carbon fibers that can be used to print cellular composites with fibers aligned in the print direction. The mechanical properties show substantial increase with aligned fibers.

2.4 Problem Statement

Various processes to align fibers and their effect on the mechanical properties have been discussed. However, research on aligning fibers in micro sized components is yet to be explored. Freeform fabrication of fiber reinforced composites has the potential to produce complex geometries with preferential alignment of fibers. Fibers can be aligned around stress concentration of a component to reduce damage (Compton & Lewis, 2014). Different process parameters such as transitional speed, nozzle diameter, fiber loading fraction, standoff distance, fiber length and pressure can be controlled to maintain the fiber alignment as they exit the nozzle. There is a need to better understand the relationships between these experimental parameter values and the resulting degree of fiber alignment.

Chapter 3: Research Methodology

In the previous chapter, freeform fabrication of fiber reinforced composite was found to be a promising method for preferentially aligning discontinuous carbon fibers. To build upon the existing research in fiber alignment, the specific aims of this research can be summarized as follows:

1. Confirm the feasibility of preferentially controlling fiber alignment during 3D printing of chopped fiber composite materials.
2. Identify factors having the greatest effect on the degree of fiber alignment.
3. Demonstrate a 3D printed component with preferentially aligned fibers along the tensile axis having superior mechanical properties to the same component in which fibers are aligned perpendicular to the tensile axis.

3.1 Materials and Equipment

All materials were printed using an nScrypt Smart Pump microextrusion system that applied pneumatic pressure to push composite inks through the selected nozzles. The nScrypt system uses Aerotech PRO115 mechanical-bearing ball-screw linear stages to move the work table in the X and Y directions as well as the deposition head in the Z-axis direction. Composite inks were loaded into 3 *c.c.* plastic syringe barrels, and the nScrypt machine supplied the specified amount of air pressure to push ink through the barrel and out of the needle tip. Luer-lock blunt dispensing needle tips were used provided by CML supply. All experiments were performed using Panex 35 milled carbon fibers from ZOLTEK Inc. The fiber diameter and the average fiber length of the carbon fibers as stated by the manufacturer were 7.2 μm and 100 μm respectively (Zoltek, http://www.zoltek.com/wp-content/uploads/2013/12/Datasheet-PX35-Milled.pdf).

For the first phase of experimentation, a clear colorless ultraviolet (UV) cure epoxy resin from Artclayworld with cure time of 30-60 seconds was used to study the fiber alignment. The carbon fibers and UV cure resin were mixed in the prescribed proportions using a Thinky ARM-310 mixer for 20 minutes before extruding. The ink was loaded into 3 *c.c.* luer-lock syringes and placed in vacuum for 1

hour to remove any bubbles induced during mixing. Lines were printed using specified parameter values. The extruded lines were subsequently cured using an Electro-Lite ELC-600 UV spot curing light source. Printed samples were examined using a Hirox KH 7700 digital microscope to observe the fiber orientation. All images were captured at 400X optical zoom under the same lighting conditions using the microscope's Multi- Focus synthesis capabilities that allow multiple images taken at different focal distances to be merged into a single "in focus" image via image processing.

For the second phase of research, ASTM D638-10 Type V tensile coupons were printed from composite ink using 3M's 2214 Non- Metallic filled thermo epoxy. Printed samples were cured at 150 °C for one hour. The tensile strength for the coupons was determined using an Instron 4301 materials testing machine. The equipment had a load cell with a capacity of 5 *KN*.

3.2 Feasibility Testing

In order to establish baseline feasibility of aligning carbon fibers in an epoxy matrix, a feasibility test was conducted as follows. A composite mixture of carbon fibers (14% by weight) with the UV cure resin was extruded through a 16 Gauge nozzle. A spiral pattern was printed on a Mylar substrate using the process parameter values shown in Table 1. Micrographs were obtained at different locations as shown in Figure 4.

Table 1: Preliminary process parameter values

Parameter	Value
Length of Carbon Fiber (Ball Mill Time)	0 sec
Nozzle Inner Diameter (Gauge)	Gauge 16 = 1.194 *mm*
Fiber Loading Fraction (*wt. %*)	14%
Air Pressure (*kPa*)	145 *kPa*
Translation Speed (*mm/sec*)	2*mm/sec*
Standoff Distance (*mm*)	2.5 *mm*

The micrographs show excellent fiber alignment parallel with the direction of nozzle travel during printing. This experiment confirmed the basic feasibility of preferential fiber alignment through control of the print parameters. This justified further experimentation to identify the significant process factors and their effects on fiber alignment.

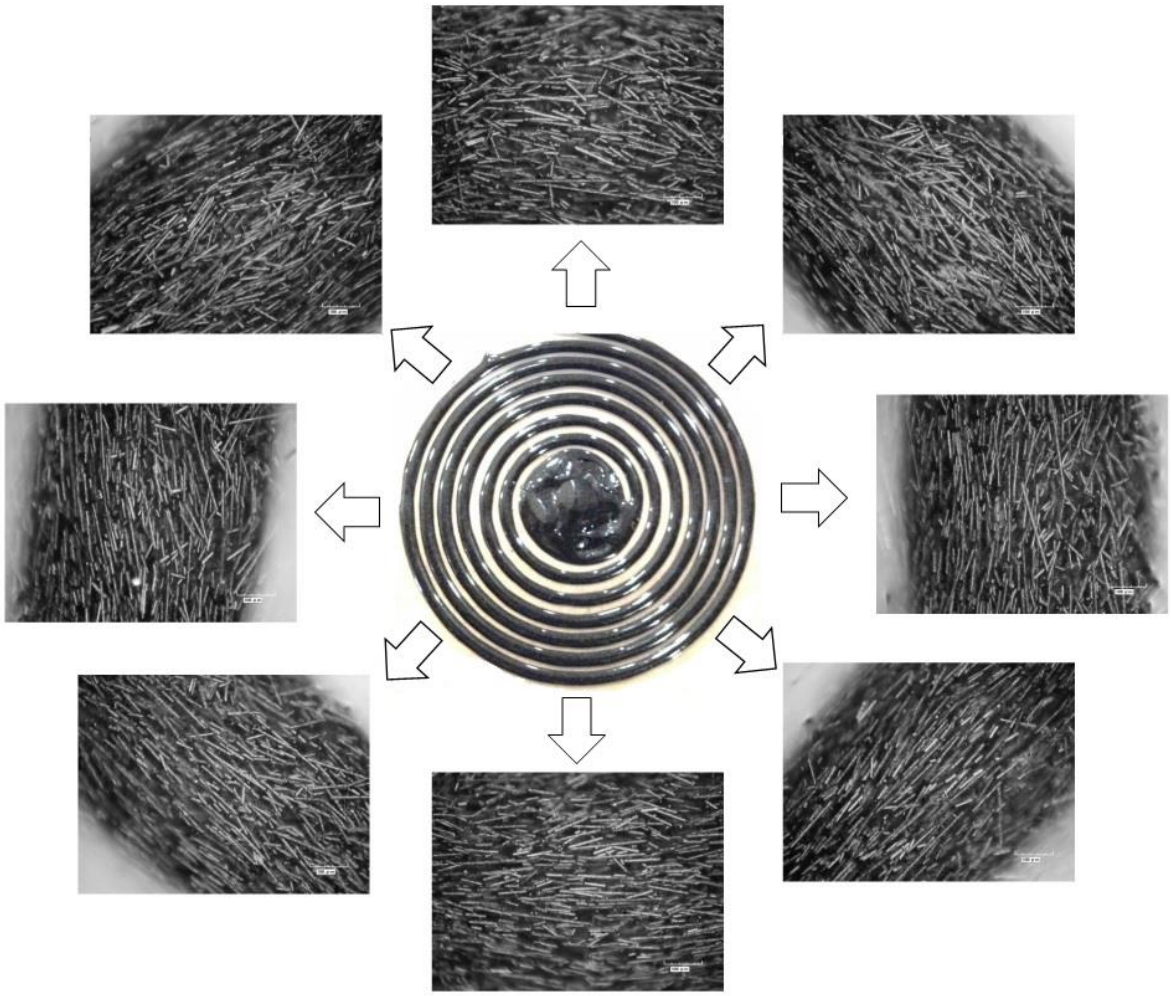

Figure 4: Spiral print to demonstrate fiber alignment parallel with the nozzle travel direction

3.3 Experimental Design to Align Carbon Fibers

Fiber alignment was observed by running a series of experiments with varied parameter settings. A 6-factor, two level half fractional factorial design (32 runs) was designed to determine which factors had the

greatest significance on fiber alignment. For every run, a straight horizontal line of composite ink was printed on a Mylar substrate with the appropriate parameter settings for that experiment. The lines were UV cured for 120 seconds after they were printed. The machine code used in the experiments is given in Appendix A. For each sample, three micrographs were obtained at three different points separated by a distance of 15*mm* as shown in Figure 5.

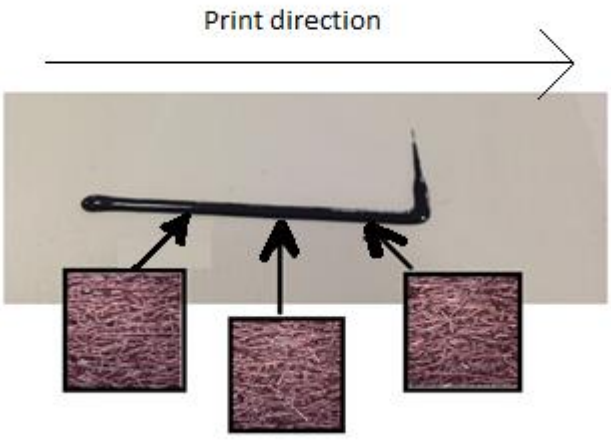

Figure 5: Sample extruded line and the micrograph locations

3.3.1 Evaluation and Measurement of Fiber Orientation

In order to quantitatively evaluate fiber orientation as the experimental response variable, a method similar to the one used by Ayres *et al.* (2008) to measure the fiber alignment in electrospun materials was adapted. It uses a Two Dimensional (2D) Fast Fourier Transform (FFT) to measure the fiber alignment. Each image is cropped to an integer power of 2 pixel dimensions (512x512, 1024x1024 pixels) and saved as a grayscale image in the TIFF graphics file format. ImageJ software supported by an oval profile plug-in was used to conduct the 2D-FFT analysis. The plug-in takes the image bounded by an oval region and samples the oval at equal angles.

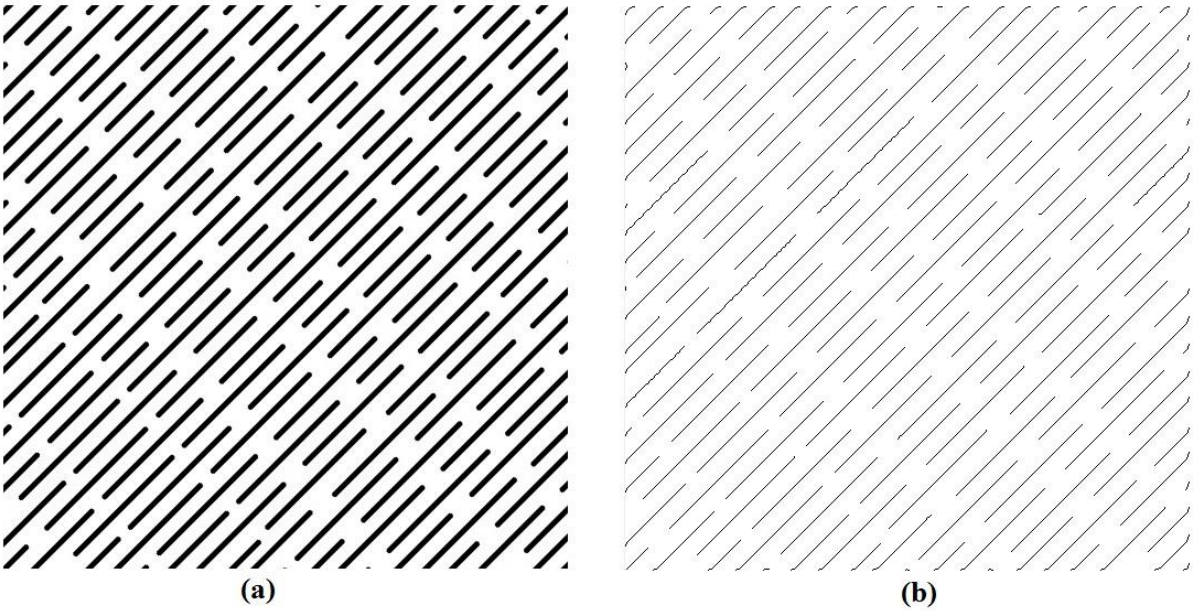

Figure 6: (a) Grayscale image (b) Skeletonized image

Figure 6(a) conceptually illustrates a grayscale image of fibers oriented at a 45 degree angle. The grayscale image is transformed into a binary image using ImageJ's "Make Binary" function *(Process/Binary/Make Binary)*. In order to preserve the extent and connectivity of fibers, the binary image is then skeletonized using ImageJ's "Skeletonize" function (*Process/Binary/Skeletonize)*. Skeletonize is used for feature extraction and representing the object's topology. Figure 6(b) shows the skeletonized version of Figure 6(a).

To obtain a 2D-FFT plot, ImageJ's "FFT" function *(Process/FFT/FFT)* is used. The 2D-FFT function converts spatial information into a mathematically defined frequency domain. This frequency domain plots the rate at which pixel intensities change in the spatial domain and produces a frequency plot composed of grayscale pixels distributed in a pattern.

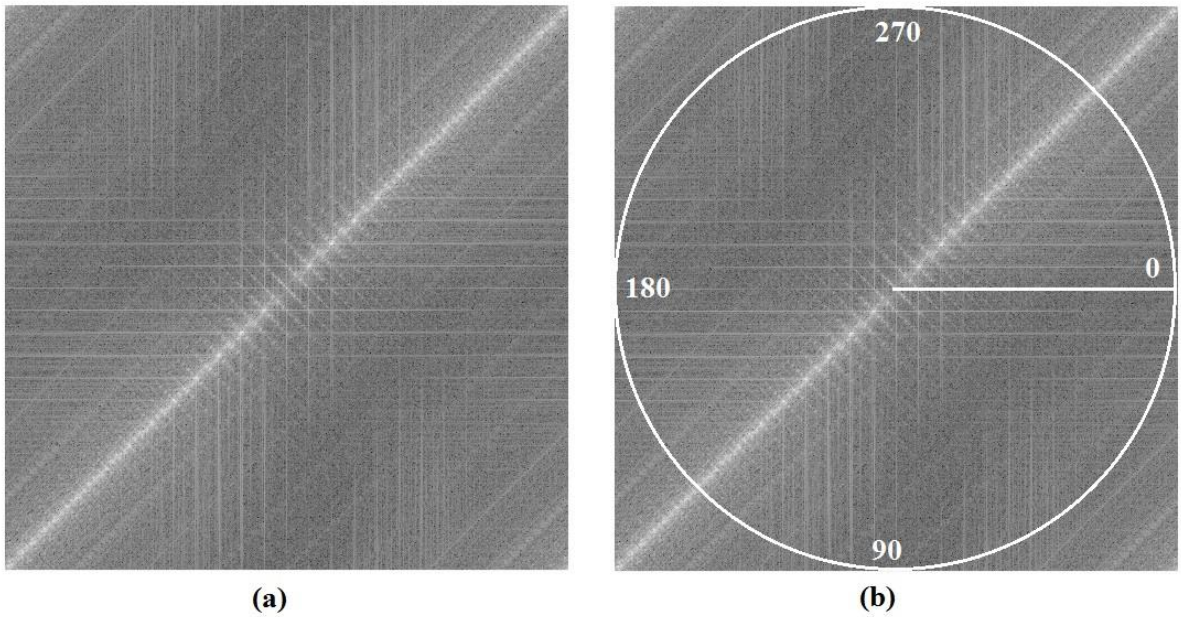

Figure 7: (a) 2D-FFT plot (b) Circular projection on frequency plot

Figure 7(a) shows the 2D-FFT frequency plot rotated to 90° for the 45 degree sloped fiber example from Figure 6(a). Note the presence of a bright stripe at 45 degrees. The distance of the stripe from the origin and the narrow width of the stripe indicate a very large percentage of pixels oriented at 45 degrees. Conversely, an FFT plot showing a white circle at the center of the plot would be characteristic of an image with entirely random fiber alignment. In Figure 7, The frequency plot is rotated to 90° to correct the rotation induced by the 2D FFT analysis. Low frequency pixels are at the center of the plot, while the high frequency pixels are placed away from the origin. A circular projection is placed on the frequency plot as seen on Figure 7 (b) using ImageJ's circular marquee tool. The ImageJ oval profile plug-in is then used to get the summed pixel intensities for each radius of the circular projection onto the FFT frequency plot. The value of summed pixel intensities for each radius is copied to Microsoft Excel to generate the 2D FFT fiber alignment plot. Table 2 illustrates the normalization process to obtain the FFT alignment value.

Table 2: Normalization process to obtain FFT alignment value

A	B	C	D	E
Fiber Angle (Degrees)	**Summed Pixel Intensity**	**Minimum Pixel Intensity Over All Fiber Angles**	**Normalized Pixel Intensity (B/C)**	**2D FFT Alignment Value (B/C)-1**
0	30296.7559	30069.3633	1.007562269	0.007562269
1	30727.5195		1.021887933	0.021887933
2	30121.0391		1.001718553	0.001718553
3	30261.0566		1.006375037	0.006375037
4	30312.3418		1.0080806	0.0080806
5	30560.7539		1.016341902	0.016341902
.	.		.	.
.	.		.	.
87	30069.3633		1	0
.	.		.	.
.	.		.	.
355	31720.2578		1.054902875	0.054902875
356	31040.8867		1.03230941	0.03230941
357	30994.1641		1.030755583	0.030755583
358	31606.4512		1.051118073	0.051118073
359	31517.2871		1.048152792	0.048152792

Column B in Table 2 shows All values are divided by the minimum alignment value of summed pixel intensity, and later subtracted by 1 to shift the alignment values to a normalized baseline value of 0. The normalized data gives the value for 2D-FFT plot ranging from 0 to approximately 0.6. The higher the alignment value is, the stronger the degree of fiber alignment is at the corresponding angle. A scatter plot of the results can be generated using Microsoft Excel. Figure 8 shows the graph from the data generated in Table 2. The peak shape and height determines the degree of alignment, while the peak position

indicates the principle axis of orientation of the fibers. A high and narrow peak indicates a uniform degree of fiber alignment at that orientation angle, whereas a shorter wider peak indicates more than one axis of alignment may be present (Ayres *et al.*, 2008).

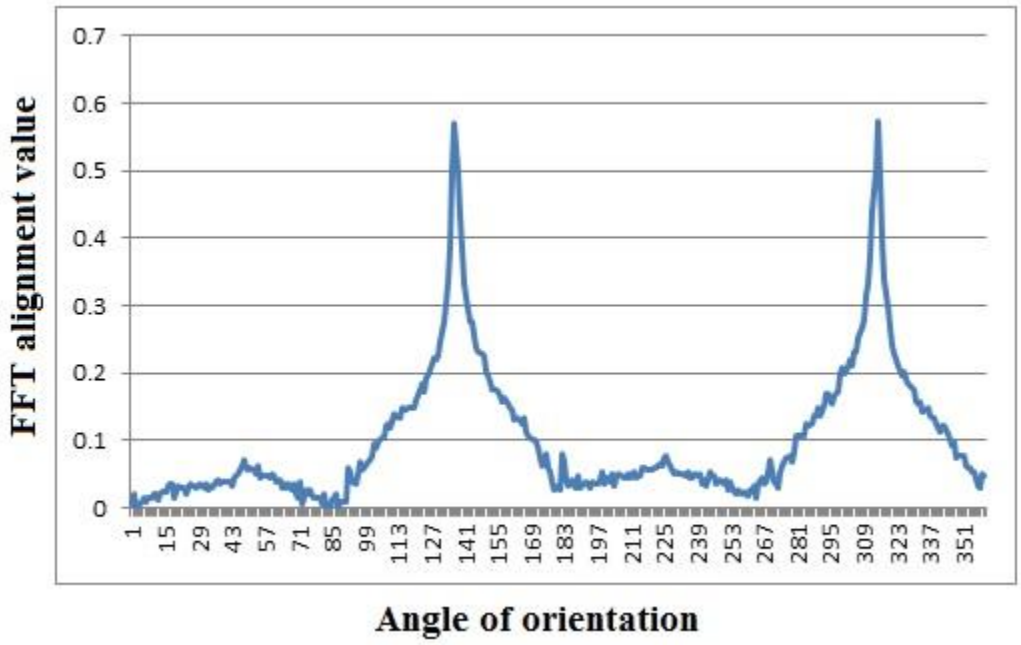

Figure 8: 2D FFT alignment plot

3.3.2 Factor Levels of Experimental Design

A large number of carbon fiber composite lines were printed on the nScrypt machine with different process parameter value settings to decide the levels for each factor. Figure 9 illustrates the schematic representation of the factors considered for experimentation:

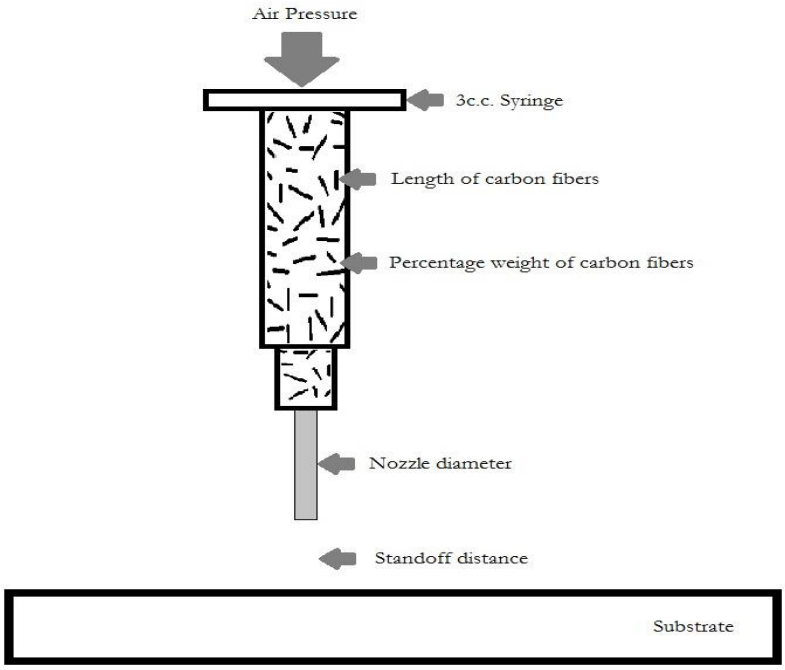

Figure 9: Micro-extrusion process with various factors

- *Standoff Distance (mm):* This is the distance between the tip of the nozzle and the print substrate. If the nozzle tip is too far above the substrate, the carbon fiber composite paste will tend to break apart into discontinuous lines, whereas the nozzle tip will plow through the extruded carbon fiber composite paste if the nozzle tip is too close to the substrate.
- *Nozzle Diameter (mm):* Various nozzle diameters with different inner diameters can be used to extrude the carbon fiber composite paste.
- *Air Pressure (kPa):* Pastes are loaded in 3 *c.c.* syringe barrels, and air pressure applied to the syringe barrel wiper controls the mass flow rate at which paste is pushed out of the needle tip. The mass flow rate increases as the air pressure increases. The lower level for the air pressure was the value where the composite ink would just barely extrude through the smallest nozzle diameter used in the experiment.

- *Fiber Loading Fraction (Wt. %):* The fiber loading fraction significantly affects the viscosity of the carbon fiber composite paste. When the percentage of carbon fiber increases, the viscosity also increases. Higher air pressure is required to extrude polymer with a high percentage weight of carbon fiber.
- *Translation Speed (mm/sec):* The cross sectional area of material deposited is inversely proportional to transitional speed. For a given paste extrusion rate, lower print head translation speeds will produce lines with greater cross sectional area. At high print head translation speeds, the printed bead of material stretches out and can even break into discontinuous line segments. The upper limit of the translation speed was determined by finding the maximum speed where the material just deposited on Mylar substrates without breaking up into discontinuous lines.
- *Length of Carbon Fibers (µm):* Purchased carbon fibers can be shortened by mechanical ball milling. The length of carbon fiber depends on the time in the ball mill. If the length of carbon fiber is too long, fiber-to-fiber interactions and entanglements in the paste dominate, thereby causing the nozzle tip to clog. If the fiber length is too small, the strength of the resulting material will not be sufficient due to the low bonding surface area between the fibers and the polymer matrix. A ball mill from Across International LLC was used to decrease the average fiber length in this research. A mass of 0.8 *gm* of carbon fibers along with 10 ceramic balls (0.125" diameter) were loaded in the mixer. To determine the lower limit for the length of fiber, four different samples were taken after running the mixer for 0, 30, 60 and 90 sec. Lengths of 250 fibers were measured for each sample. Figure 10 shows a histogram of carbon fiber length for the corresponding ball milling time.

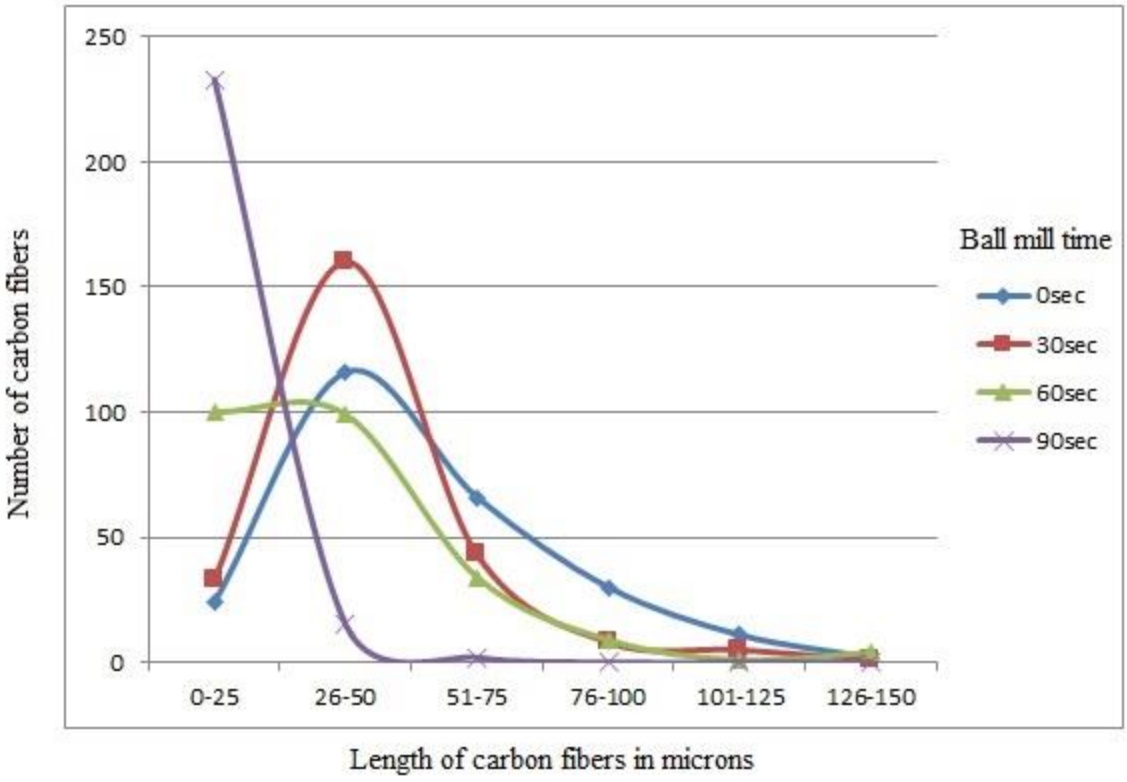

Figure 10: Length of carbon fibers for corresponding ball milling time

Using the above process parameter definitions, preliminary experiments were conducted to identify suitable upper and lower parameter values for subsequent formal DOE trials. Table 3 shows the upper and lower factor levels considered for the factorial design.

Table 3: Factor levels of experimental design

Factor	Upper limit	Lower limit
Length of Carbon Fiber (as indicated by ball mill time in sec.)	0 sec	90 sec
Nozzle Inner Diameter (*mm*)	Gauge 16 = 1.194 *mm*	Gauge 19 = 0.686 *mm*
Fiber Loading Fraction (*Wt. %*)	15%	5%
Air Pressure (*kPa*)	165*kPa*	145*kPa*
Translation Speed (*mm/sec*)	2 *mm/sec*	0.5 *mm/sec*
Standoff Distance (*mm*)	2.5 *mm*	1.25 *mm*

3.4 Test Method for Tensile Properties

To study the effect of fiber alignment on mechanical properties of the 3D printed composite test samples, tensile properties of printed samples were measured as per ASTM D638-10, 2013. Two sets of five samples each were printed, one with fibers aligned along the tensile axis and the other with fibers perpendicular to tensile axis. The machine code used in the experiments is given in Appendix A. The pastes used in this preliminary research tended to sag somewhat after printing, hence the carbon fiber composite paste was printed inside a mold in the directions as shown in Figure 11. Future research will make use of newer no-sag thermal cure epoxies to eliminate any need for the containment mold.

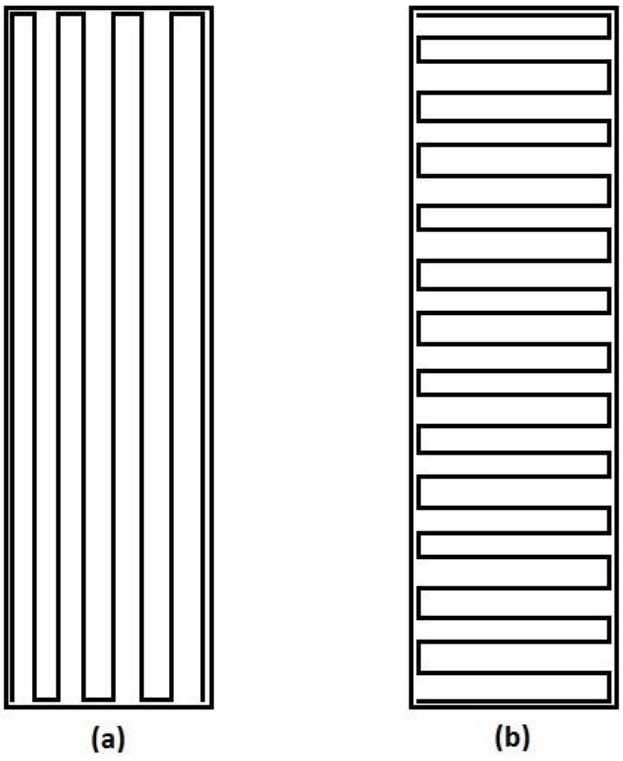

Figure 11 (a) Print direction along the tensile axis. (b) Print direction perpendicular to tensile axis

Figure 12 shows the dimensions of the mold. A 3 *c.c.* luer-lock plastic syringe barrel was loaded with the carbon fiber epoxy composite paste and was placed in vacuum to remove air bubbles. The mold was made of three plates; the bottom and middle plate were fastened while printing, whereas the top plate was

fastened after all layers were printed. All three plates were coated with Mann Ease Release 200 mold spray. The mold release was allowed to air dry for 15 minutes before printing on the nScrypt machine. After each new layer of carbon epoxy paste was printed, the z-height of the nozzle was increased with respect to the last layer by an amount equal to the standoff distance specified for that experiment. Four layers were printed in total to reach the desired tensile bar thickness. After all layers were printed, the top plate was fastened, and the entire mold was kept in an oven at 150 °C for 1 hour in order to cure the epoxy. Figure 13 shows the extrusion process of the composite ink into the mold.

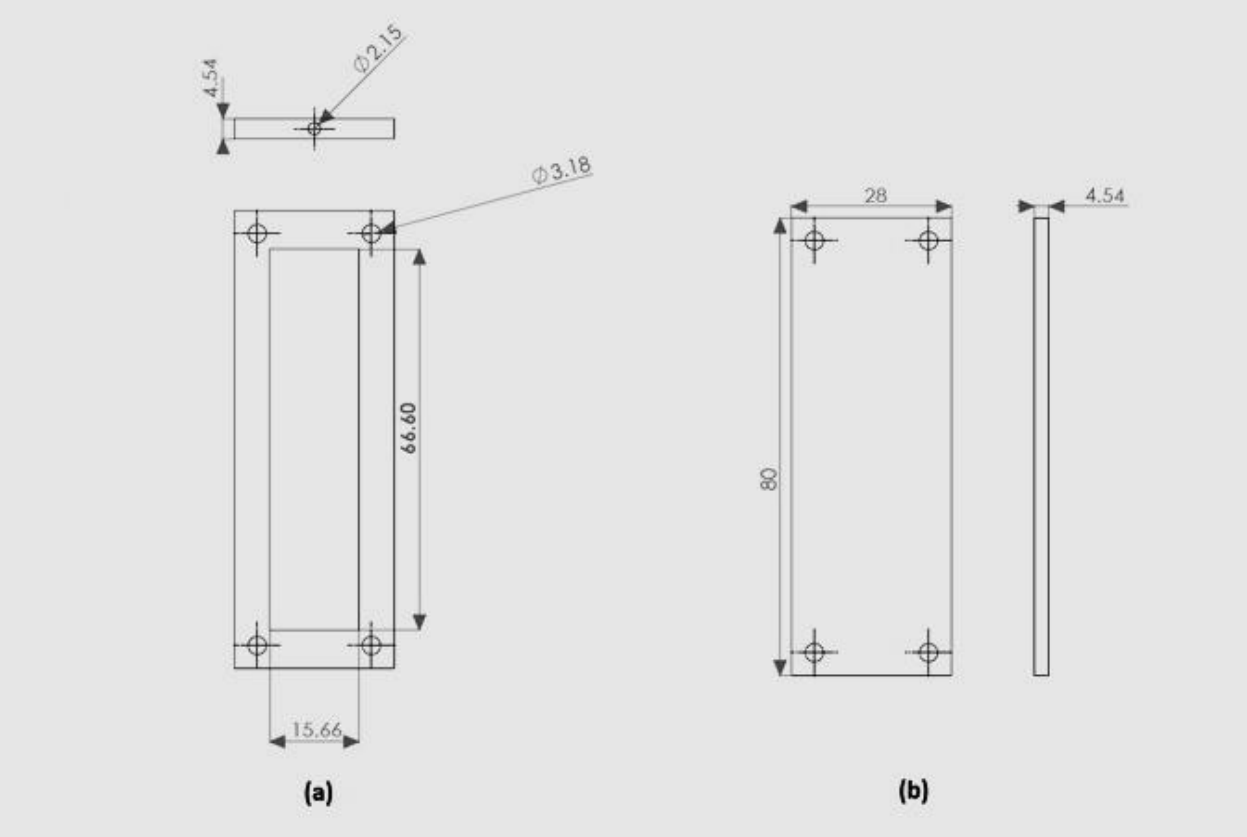

Figure 12: Dimensions of the mold. Figure (a): Middle plate. Figure (b): Top and bottom plate

Figure 13: Extrusion of composite in the mold

After thermally curing the epoxy, the part was removed from the mold and was milled from all sides to create flat surfaces for reliable tensile test results. A thickness of 2.8 *mm* was maintained on all the samples. A Flow Mach 2 waterjet machine was used to machine the ASTM D638-10, type 5 tensile coupon profiles on the milled samples as seen in Figure 14. Figure 15 shows the dimensions for ASTM D638-10, type 5 coupons.

Figure 14: ASTM D638-10, Type 5 profile using waterjet machining

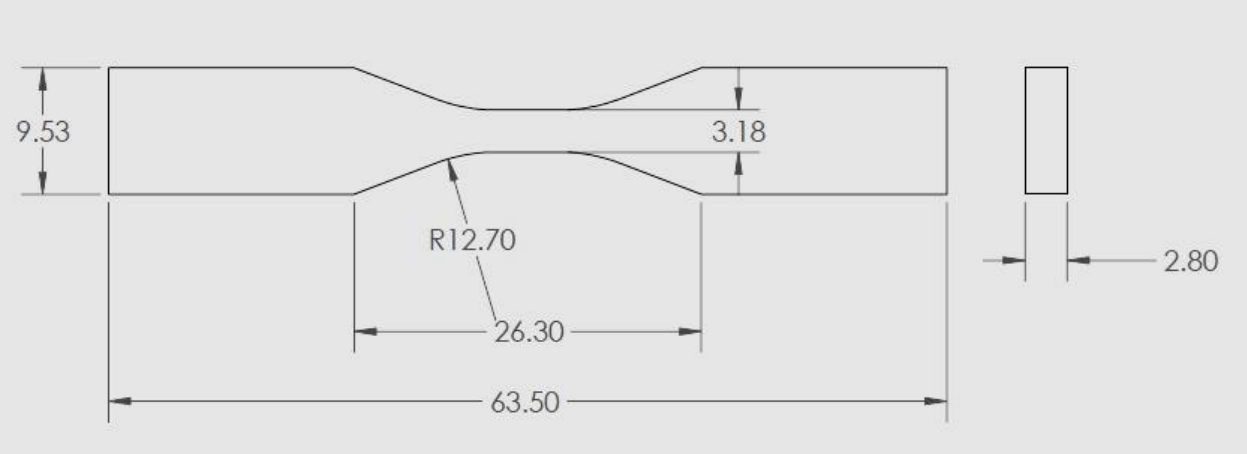

Figure 15: Dimensions for ASTM D638-10, Type 5. 2013

Chapter 4: Experimental Results and Analysis

As proposed in Section 1.5, one of the thesis objectives was to find the significant factors affecting carbon fiber alignment. A second objective was to demonstrate the ability to build up 3D structures with aligned fibers and to measure the effect of fiber alignment on tensile strength.

4.1 Design of Experiments

Minitab 17 statistical software was used to generate a 6-factor, half fractional factorial design with 32 runs. FFT fiber alignment values for each run were obtained using the methods described in Section 3.3.1. Since a horizontal line was extruded for each run, the FFT fiber alignment value was determined at an angle of 180. To take into account any variation that may have been induced in micrograph images while printing and capturing image, the FFT fiber alignment value was determined by the highest value at angle 180±2°. The average of FFT fiber alignment value at three different positions for a given line was used as the experimental response variable. Table 4 shows the design table and data for the design of experiments. Figure 16 shows the selection of highest FFT alignment value for run order 4 (position3) from Table 4 with respect to the print orientation.

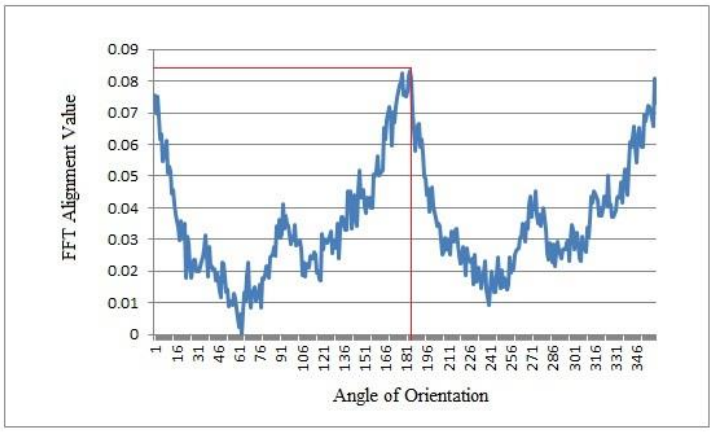

Angle	Summed Pixel Intensity	Normalization Value	Intensity/ Normalization	2D FFT Alignment Value
178	75188.45	69907.56	1.0755	0.0755
179	75290.27	69907.56	1.0770	0.0770
180	75157.25	69907.56	1.0751	0.0751
181	75274.15	69907.56	1.0768	0.0768
182	75617.68	69907.56	1.0817	0.0817

Figure 16: Selection of FFT alignment value to corresponding angle of orientation

Table 4: Design table and data for design of experiment

Run Order	% C	Length	Speed	Pressure	Nozzle dia.	Stand-off	FFT 1	FFT 2	FFT 3	AVG FFT
1	-1	-1	1	-1	1	-1	0.063	0.063	0.038	0.055
2	1	1	1	1	-1	-1	0.099	0.113	0.092	0.101
3	1	-1	-1	-1	1	-1	0.030	0.040	0.068	0.046
4	1	1	-1	-1	-1	-1	0.076	0.100	0.082	0.086
5	-1	-1	-1	1	-1	1	0.067	0.045	0.064	0.059
6	1	-1	1	1	-1	1	0.075	0.096	0.063	0.078
7	-1	1	1	1	1	-1	0.051	0.065	0.030	0.049
8	-1	-1	1	-1	-1	1	0.091	0.104	0.123	0.106
9	1	-1	-1	1	-1	-1	0.076	0.050	0.056	0.060
10	1	-1	-1	-1	-1	1	0.048	0.043	0.060	0.050
11	-1	1	1	1	-1	1	0.071	0.058	0.061	0.064
12	1	1	-1	1	1	-1	0.052	0.028	0.052	0.044
13	-1	1	-1	-1	-1	1	0.067	0.046	0.058	0.057
14	-1	1	1	-1	1	1	0.077	0.071	0.090	0.079
15	1	1	1	-1	-1	1	0.094	0.069	0.102	0.088
16	-1	1	1	-1	-1	-1	0.146	0.114	0.087	0.116
17	-1	-1	1	1	-1	-1	0.081	0.070	0.072	0.074
18	-1	-1	-1	-1	1	1	0.028	0.039	0.041	0.036
19	1	1	1	1	1	1	0.091	0.107	0.089	0.096
20	1	1	-1	-1	1	1	0.061	0.082	0.057	0.067
21	-1	-1	-1	1	1	-1	0.044	0.043	0.036	0.041
22	-1	1	-1	-1	1	-1	0.045	0.030	0.039	0.038
23	1	-1	1	1	1	-1	0.111	0.092	0.093	0.099
24	-1	-1	-1	-1	-1	-1	0.058	0.055	0.059	0.057
25	1	-1	-1	1	1	1	0.096	0.091	0.107	0.098
26	1	-1	1	-1	1	1	0.028	0.036	0.019	0.028
27	1	1	1	-1	1	-1	0.127	0.092	0.082	0.100
28	-1	-1	1	1	1	1	0.083	0.063	0.093	0.080
29	1	-1	1	-1	-1	-1	0.071	0.087	0.049	0.069
30	-1	1	-1	1	1	1	0.042	0.047	0.034	0.041
31	1	1	-1	1	-1	1	0.086	0.096	0.099	0.094
32	-1	1	-1	1	-1	-1	0.042	0.037	0.053	0.044

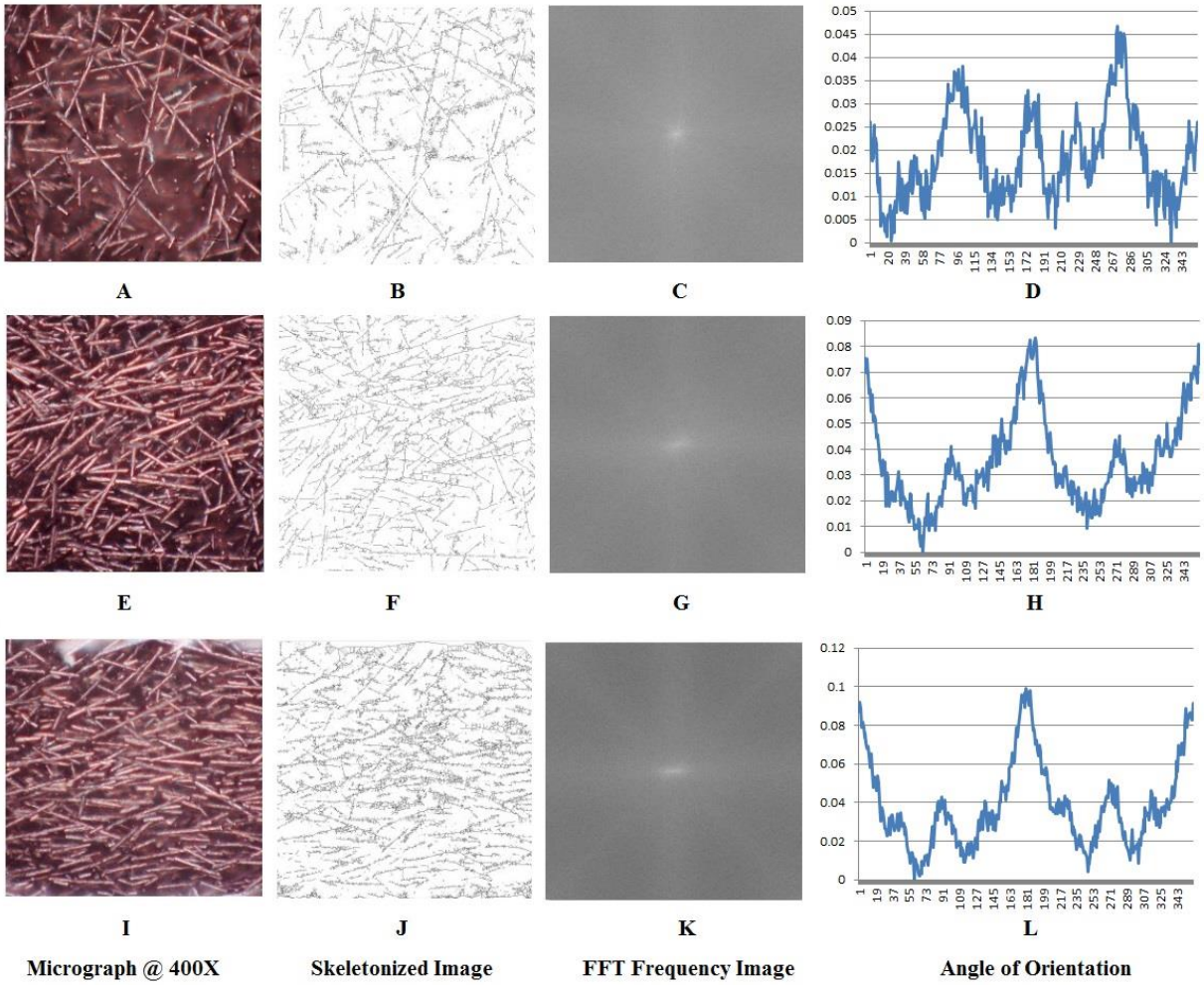

Figure 17: 2D FFT analysis of micrograph @ 400X. Images (B, F, J) are skeletonized images; Images (C, G, K) are frequency plots. Images (D, H, L) are 2D FFT alignment plots for corresponding micrograph (A, E, I)

Figure 17 shows representative samples to illustrate differences in carbon fiber alignment under varying process parameter values. Figures 17A, 17E, and 17I show micrographs for run order 7, 4, and 31 respectively from Table 4.

4.2 Analysis of Preliminary Results

Minitab 17 was used to analyze the factorial data. The detailed Analysis of Variance (ANOVA) table is given in Appendix B. The model from Appendix B was further improved by reducing the model which

would provide a better estimate for the error term by increasing the degrees of freedom associated with it. From the half normal plot in Figure 18 and the ANOVA table (Appendix B), terms for the reduced model were determined. Factor A (*Fiber Loading Fraction*), Factor B (*Length of Carbon Fibers*), Factor C (*Translation Speed*), Factor D (*Air Pressure*), Factor E (*Nozzle Diameter*), the interaction of factors A&D (*Fiber Loading Fraction and Air Pressure*) and the interaction of factors B&D (*Length of Carbon Fibers and Air Pressure*) were considered for the reduced model. The ANOVA for the reduced model is provided in Table 5.

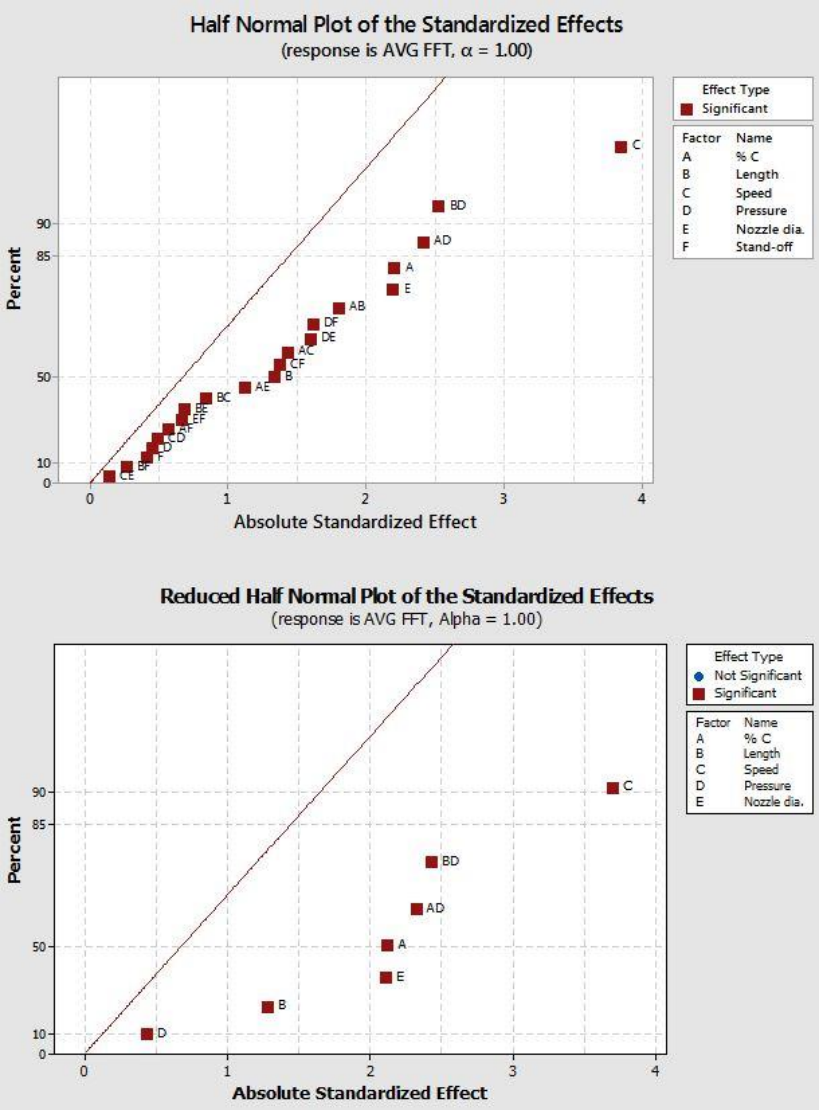

Figure 18: Half normal plots for avg. FFT alignment value

Table 5: Analysis of variance for the reduced model

Analysis of Variance

Source	DF	Adj SS	Adj MS	F-Value	P-Value
Model	7	0.010890	0.001556	5.09	0.001
Linear	5	0.007457	0.001491	4.88	0.003
% C	1	0.001383	0.001383	4.53	0.044
Length	1	0.000509	0.000509	1.67	0.209
Speed	1	0.004134	0.004134	13.53	0.001
Air Pressure	1	0.000060	0.000060	0.20	0.662
Nozzle Dia.	1	0.001371	0.001371	4.49	0.045
2-Way Interactions	2	0.003433	0.001716	5.62	0.010
% C*Air Pressure	1	0.001622	0.001622	5.31	0.030
Length*Air Pressure	1	0.001811	0.001811	5.93	0.023
Error	24	0.007333	0.000306		
Total	31	0.018223			

From the ANOVA in Table 5, it is clear that factors A (*Fiber Loading Fraction*), C (*Translation Speed*), E (*Nozzle Diameter*), and the interaction of factors A&D (*Fiber Loading Fraction and Air Pressure*) and interaction of factors B&D (*Length of Carbon Fiber and Air Pressure*) were significant with a p-value less than 0.05.

From Figure 19, the 'Residual Versus Fits' plot did not indicate any abnormalities in the variance, thus satisfying the equal variance assumption. The 'Residual Versus Order' exhibits no pattern, satisfying the independence assumption of our ANOVA model. The normal probability plot and histogram revealed normality of the residuals. The normal distribution of the variances was verified using the Anderson-Darling test for normality. Figure 20 shows a normal probability plot of the residuals with a goodness of fit test. The p-value obtained was 0.843 which is greater than 0.05, hence it was concluded that the residuals were normally distributed.

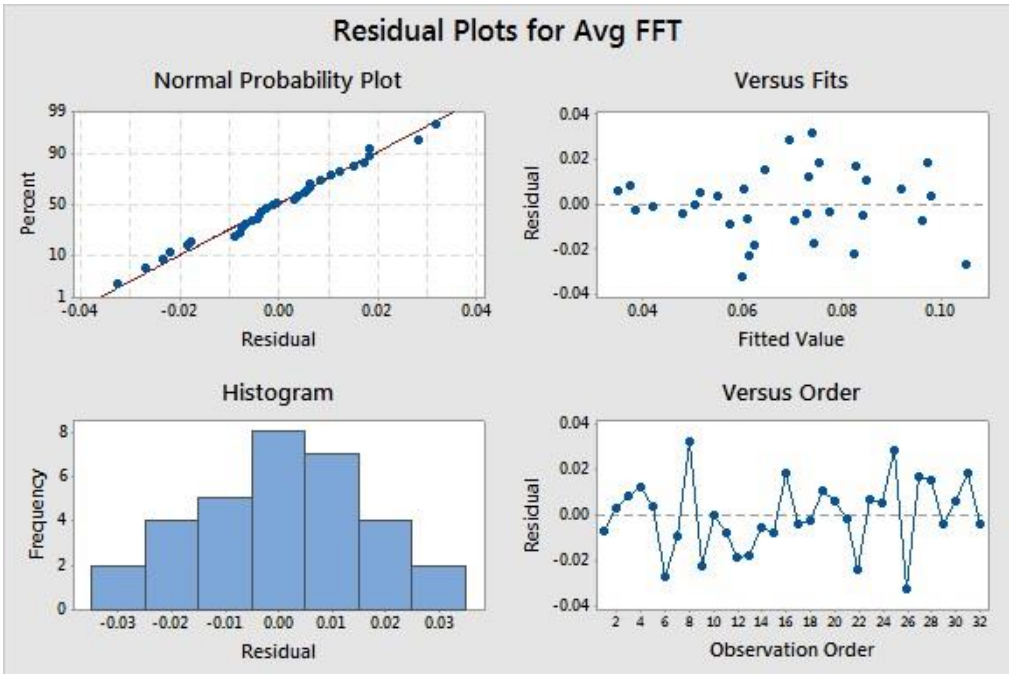

Figure 19: Residual plots for avg. FFT alignment value

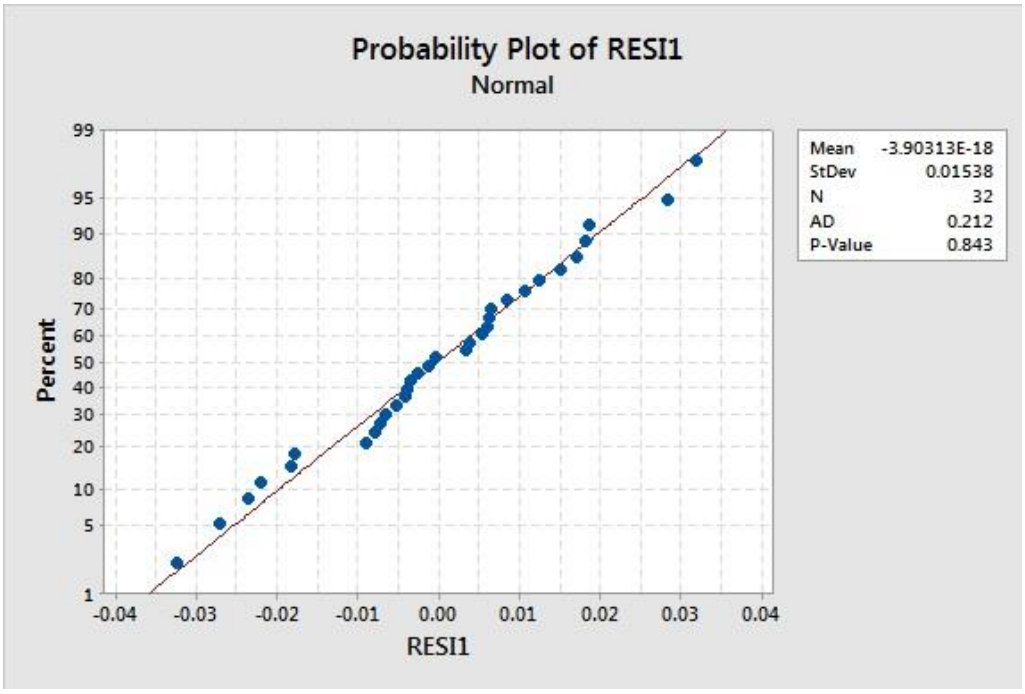

Figure 20: Normality test for residuals from avg. FFT alignment value

The main effect plot from Figure 21 shows the optimal value for the significant factors A (*Fiber Loading Fraction*), C (*Translation Speed*) and E (*Nozzle Diameter*). To maximize the degree of fiber alignment, the fiber loading fraction should be high (15 *Wt. %*), the translation speed should be high (2 *mm/sec*), and a nozzle gauge should be low (Gauge 19).

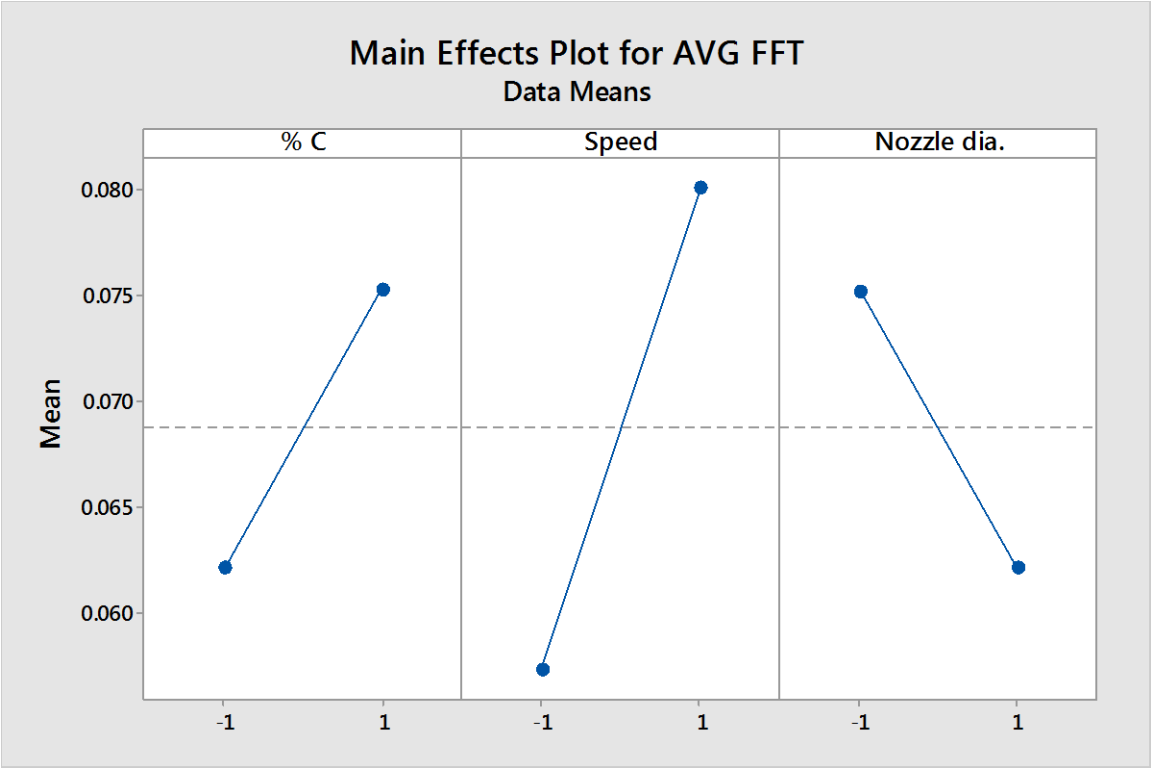

Figure 21: Main effects plot for avg. FFT alignment value

Figure 22 shows the 2-Way interaction plot for the significant factors A&D (*Fiber Loading Fraction and Air Pressure*) and factors B&D (*Length of Carbon Fibers and Air Pressure*). From the graph between fiber loading fraction and air pressure, it is observed that to maximize the degree of fiber alignment, fiber loading fraction and air pressure should be high (15%, 165 *kPa* respectively). Similarly, from graph between length of carbon fibers and air pressure, it is observed that higher value for length of carbon fibers and lower value for air pressure leads to better fiber alignment. Due to a small difference between the effect value at high length-low pressure (0.078) and low length-high pressure (0.073), the optimum

run conditions were chosen at low length- high pressure as it complements the results obtained from interaction between fiber loading fraction and air pressure.

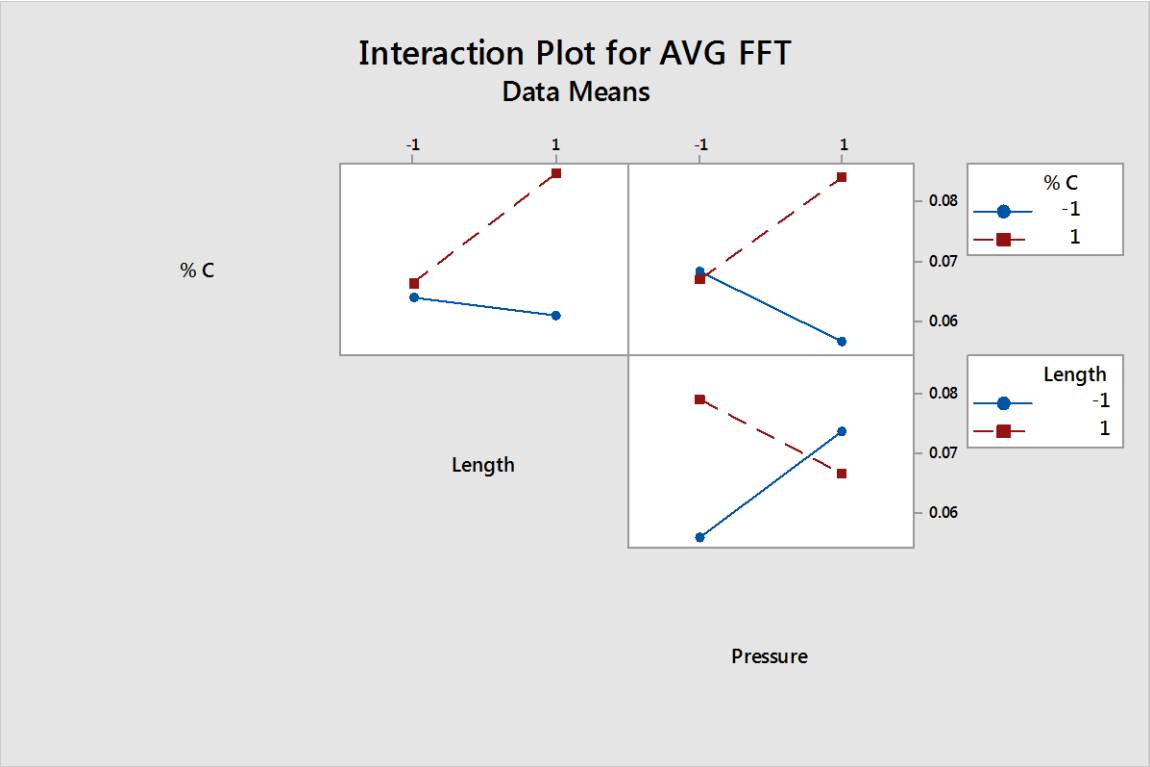

Figure 22: Interaction plot for avg. FFT alignment value

Comments:

For practical applications, UV cure resin cannot be used with the carbon fibers to print a functional part, as the resin doesn't cure to its full depth. Carbon fiber blocks the UV light which leaves behind uncured resin at the bottom of the printed line. The main purpose of using a clear colorless ultraviolet (UV) cure resin for the experiment was to obtain clear images of the fibers and to analyze their orientation at three locations as described in Section 3.3. For real world applications, a UV cure resin can be replaced with a no-sag thermal cure epoxy. Also, as observed by Kuriger *et al.* (2001), tensile strength increases as fiber length increases.

4.3 Effect of Aligned Fibers on Mechanical Properties

To attain optimal carbon fiber alignment in the tensile coupons, the recommended parameter settings from Section 4.2 were used when printing samples.

- *Translation Speed & Fiber Loading Fraction:* As observed from the main effects plot (Figure 21), the degree of fiber alignment improves with higher translation speed and carbon fiber loading fraction. So the speed used to extrude the epoxy was 2 *mm/sec* with 15 *wt. %* of carbon fibers.
- *Nozzle Diameter & Air Pressure:* From the main effect plot (Figure 21) and interaction plot (Figure 22), a higher level for nozzle gauge number and air pressure leads to better fiber alignment. However, as the viscosity of thermal cure epoxy is higher than that of UV cure polymer, optimal values failed to extrude the composite paste. An 18 gauge nozzle was therefore chosen, and pressure was increased to 290 *kPa*, which are the highest values at which the process can be carried out.
- *Length of Carbon Fibers:* To observe the effect of aligned fibers on mechanical strength, long fibers were considered. As observed in Figure 10, the fiber length at ball mill time of 0 sec were long, hence carbon fibers at ball mill time 0 sec were used.
- *Standoff Distance:* The lower level of the stand-off distance (1.25 *mm*) was used.

The printed and cured tensile samples were loaded in the test fixture jaws, and a distance of 25.4 *mm* was maintained between the two grips. A cross head speed of 25 *mm/min* speed was used on all samples. The software generated a report with all tensile testing data and the stress strain curves.

Results:

From Figures 23 and 24, a significant difference in the ultimate tensile stress and modulus was observed depending on the fiber orientation. Mechanical properties of the composite with fibers along the tensile

axis were greater as compared to the fibers perpendicular to the tensile axis. The variability observed along the axis may be induced because of the milling operation performed on the cured part.

The average ultimate tensile stress increased by 44.12% from $4.6033*10^4$ *kPa* for samples with fibers perpendicular to tensile axis to $6.6341*10^4$ *kPa* for samples with fibers along the tensile axis. The average modulus increased by 42.67% from $2.8383*10^6$ *kPa* for samples with fibers perpendicular to tensile axis to $4.0493*10^6$ *kPa* for samples with fibers along the tensile axis.

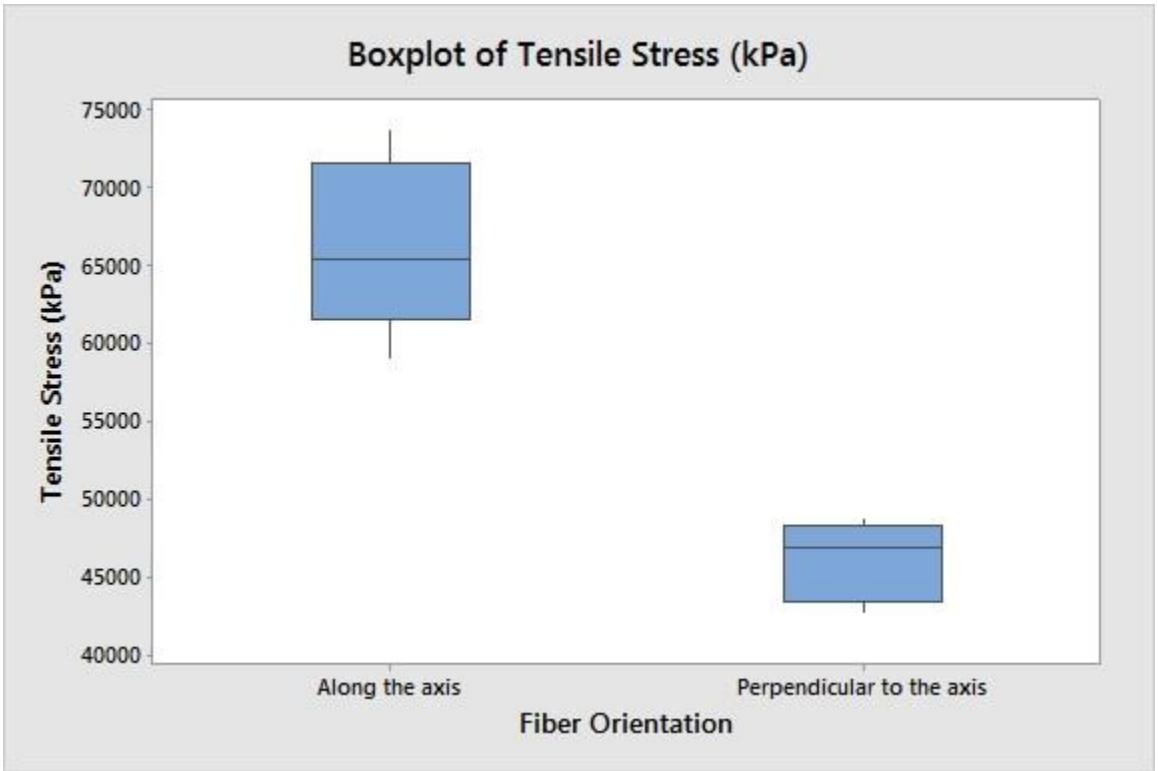

Figure 23: Boxplot of tensile stress

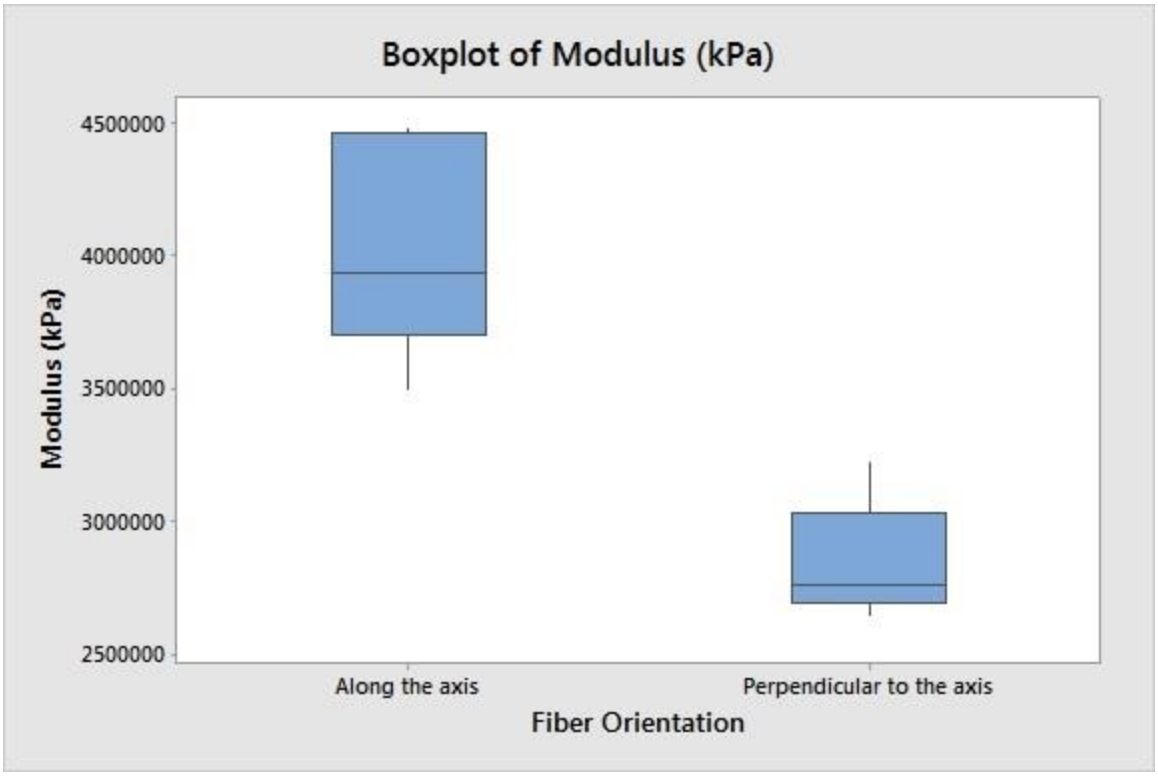

Figure 24: Boxplot of modulus

Chapter 5: Conclusions and Recommendations

5.1 Summary

The ability to print a composite ink with aligned fibers was successfully demonstrated. The experimental factors found to be most significant with respect to carbon fiber alignment in micro extruded composite inks were determined using a factorial experiment. The percentage of carbon fibers, translation speed, and nozzle diameter were found to have the most significant effect on the degree of fiber alignment. It was also found that the interaction of percentage of carbon fibers with pressure and interaction of length with pressure were also significant. The optimal levels for these factors were determined using the main effects plot and interaction plot. Since a UV cure resin limits the thickness of carbon fiber epoxy paste that can be cured while printing a functional part, a thermal cure epoxy temperature was proposed.

The mechanical properties of the printed part with carbon fibers aligned along and perpendicular to tensile axis were also studied. Tensile coupons for the two fiber orientations were tested. The results showed 44.11% increase in ultimate tensile stress, and a 42.66% increase in modulus for the samples with carbon fibers aligned along the tensile axis.

5.2 Recommendations for Future Work

In this research study, carbon fiber loading fraction was limited to 15% by weight. Higher loading fraction of carbon fiber can be used to increase the tensile strength and stiffness of the part. Different ways to increase fiber loading without affecting fiber alignment must be investigated. Length of carbon fiber is also a decisive factor as it affects fiber alignment as well as the mechanical properties. The strength of the composite reaches its maximum potential when the length of carbon fibers meets the critical fiber length. Different ways to extrude longer fibers which satisfy the critical fiber length without clogging the nozzle must be studied.

The current research focuses on fiber alignment only in X and Y plane. Different methods to induce fiber orientation in the Z- axis direction and its effect on the mechanical properties must be explored.

A Computer-Aided Analysis algorithm to determine preferred fiber orientations to resist mechanical loading and minimize damage will be useful. Development of such an algorithm which can be used as an add-on with any CAD software to provide output in a file format that can be sliced by a 3D printer software. Similarly, a slicing software algorithm that takes the CAD result and generates a toolpath that will lay down fibers in the preferred orientation can be developed.

References:

ASTM D638 - 10 Standard Test Method for Tensile Properties of Plastics, PA 19428-2959, 2013

Ayres, C. E., Jha, B. S., Meredith, H., Bowman, J. R., Bowlin, G. L., Henderson, S. C., & Simpson, D. G. (2008). Measuring fiber alignment in electrospun scaffolds: a user's guide to the 2D fast Fourier transform approach. *Journal of Biomaterials Science, Polymer Edition, 19*(5), 603-621.

Bagherpour, S. (2012). Fibre Reinforced Polyester Composites.

Calvert, P., Lin, T. L., & Martin, H. (1997). Extrusion freeform fabrication of chopped-fibre reinforced composites. *High Performance Polymers, 9*(4), 449-456.

Campbell, F. C. (2010). *Structural Composite Materials*: Asm international.

Chung, D. D. L. (1994). *Carbon fiber composites*: Butterworth-Heinemann.

Compton, B. G., & Lewis, J. A. (2014). 3D-Printing of Lightweight Cellular Composites. *Advanced Materials*.

Crowson, R., Folkes, M., & Bright, P. (1980). Rheology of short glass fiber-reinforced thermoplastics and its application to injection molding I. Fiber motion and viscosity measurement. *Polymer Engineering & Science, 20*(14), 925-933.

Fu, S.-Y., & Lauke, B. (1996). Effects of fiber length and fiber orientation distributions on the tensile strength of short-fiber-reinforced polymers. *Composites Science and Technology, 56*(10), 1179-1190.

Hughes, M. P. (2000). AC electrokinetics: applications for nanotechnology. *Nanotechnology, 11*(2), 124.

Kim, G., Moeller, D., & Shkel, Y. (2004). Orthotropic polymeric composites with microstructure tailored by electric field. *Journal of composite materials, 38*(21), 1895-1909.

Kim, G. H., & Shkel, Y. M. (2004). Polymeric composites tailored by electric field. *Journal of materials research, 19*(04), 1164-1174.

Kuriger, R. J., Alam, M. K., & Anderson, D. P. (2001). Strength prediction of partially aligned discontinuous fiber-reinforced composites. *Journal of Materials Research, 16*(01), 226-232.

Lee, K., Cheng, H., Jou, W., Chen, G., & Liang, C. (2007). The influence of carbon fiber orientation on the mechanical and tribological behavior of carbon fiber/LCP composites. *Materials chemistry and physics, 102*(2), 187-194.

Lee, S., Yang, D., Ko, J., & Youn, J. (1997). Effect of compressibility on flow field and fiber orientation during the filling stage of injection molding. *Journal of materials processing technology, 70*(1), 83-92.

Matsuoka, T., Takabatake, J. I., Inoue, Y., & Takahashi, H. (1990). Prediction of fiber orientation in injection molded parts of short-fiber-reinforced thermoplastics. *Polymer Engineering & Science, 30*(16), 957-966.

Peng, J., Lin, T. L., & Calvert, P. (1999). Orientation effects in freeformed short-fiber composites. *Composites Part A: Applied Science and Manufacturing, 30*(2), 133-138. doi: 10.1016/S1359-835X(98)00110-9

Pethig, R., & Markx, G. H. (1997). Applications of dielectrophoresis in biotechnology. *Trends in biotechnology, 15*(10), 426-432.

Pohl, H. A., & Crane, J. S. (1971). Dielectrophoresis of cells. *Biophysical Journal, 11*(9), 711-727.

Shokri, P., & Bhatnagar, N. (2012). Effect of the Post-Filling Stage on Fiber Orientation at the Mid-Plane in Injection Molding of Reinforced Thermoplastics. *Physics Procedia, 25*, 79-85.

Van den Ende, D., Van Kempen, S., Wu, X., Groen, W., Randall, C., & Van der Zwaag, S. (2012). Dielectrophoretically structured piezoelectric composites with high aspect ratio piezoelectric particles inclusions. *Journal of Applied Physics, 111*(12), 124107.

Appendix A: nScrypt machine code

Code to Extrude Composite

```
relative                        //uses relative measurement system for this file
pen SMARTPUMP_1                 //selects the nScrypt SMARTPUMP as the printing tool
speed 2                         //sets a value for the feed rate to 2 mm/s
move   60      0       0        //moves to coordinates X= 60 mm, Y=0, and Z=0
move   0       25      0        //moves to coordinates X= 0 mm, Y=25mm, and Z=0
```

Code to Cure the Extruded Line

```
relative                        //uses relative measurement system for this file
pen SMARTPUMP_1                 //selects the nScrypt SMARTPUMP as the printing tool
speed 0.5                       //sets a value for the feed rate to 0.5 mm/s
move   60      0       0        //moves to coordinates X= 60 mm, Y=0, and Z=0
move   0       25      0        //moves to coordinates X= 0 mm, Y=25mm, and Z=0
```

Code to Extrude Composite Along the Tensile Axis

```
relative
pen     SMARTPUMP_1
speed 2
move   0       65      0
move   0.5     0       0
move   0       -65     0
move   0.5     0       0
move   0       65      0
move   0.5     0       0
move   0       -65     0
move   0.5     0       0
move   0       65      0
move   0.5     0       0
move   0       -65     0
move   0.5     0       0
move   0       65      0
move   0.5     0       0
move   0       -65     0
move   0.5     0       0
move   0       65      0
```

move	0.5	0	0
move	0	-65	0
move	0.5	0	0
move	0	65	0
move	0.5	0	0
move	0	-65	0
move	0.5	0	0
move	0	65	0
move	0.5	0	0
move	0	-65	0
move	0.5	0	0
move	0	65	0
move	0.5	0	0
move	0	-65	0
move	0.5	0	0
move	0	65	0
move	0.5	0	0
move	0	-65	0
move	0.5	0	0
move	0	65	0
move	0.5	0	0
move	0	-65	0
move	0.5	0	0
move	0	65	0
move	0.5	0	0
move	0	-65	0
move	0.5	0	0
move	0	65	0
move	0.5	0	0
move	0	-65	0
move	0.5	0	0
move	0	65	0
move	0.5	0	0
move	0	-65	0
move	0.5	0	0
move	0	65	0
move	0.5	0	0
move	0	-65	0
move	0.5	0	0
move	0	65	0
move	0.5	0	0
move	0	-65	0

```
move    0.5     0       0
move    0       65      0
```

Code to Extrude Composite Perpendicular to Tensile Axis

```
relative
pen     SMARTPUMP_1
speed 2

move    15      0       0
move    0       0.5     0
move    -15     0       0
move    0       0.5     0
move    15      0       0
move    0       0.5     0
move    -15     0       0
move    0       0.5     0
move    15      0       0
move    0       0.5     0
move    -15     0       0
move    0       0.5     0
move    15      0       0
move    0       0.5     0
move    -15     0       0
move    0       0.5     0
move    15      0       0
move    0       0.5     0
move    -15     0       0
move    0       0.5     0
move    15      0       0
move    0       0.5     0
move    -15     0       0
move    0       0.5     0
move    15      0       0
move    0       0.5     0
move    -15     0       0
move    0       0.5     0
move    15      0       0
move    0       0.5     0
move    -15     0       0
move    0       0.5     0
move    15      0       0
```

move	0	0.5	0
move	-15	0	0
move	0	0.5	0
move	15	0	0
move	0	0.5	0
move	-15	0	0
move	0	0.5	0
move	15	0	0
move	0	0.5	0
move	-15	0	0
move	0	0.5	0
move	15	0	0
move	0	0.5	0
move	-15	0	0
move	0	0.5	0
move	15	0	0
move	0	0.5	0
move	-15	0	0
move	0	0.5	0
move	15	0	0
move	0	0.5	0
move	-15	0	0
move	0	0.5	0
move	15	0	0
move	0	0.5	0
move	-15	0	0
move	0	0.5	0
move	15	0	0
move	0	0.5	0
move	-15	0	0
move	0	0.5	0
move	15	0	0
move	0	0.5	0
move	-15	0	0
move	0	0.5	0
move	15	0	0
move	0	0.5	0
move	-15	0	0
move	0	0.5	0
move	15	0	0
move	0	0.5	0
move	-15	0	0

move	0	0.5	0
move	15	0	0
move	0	0.5	0
move	-15	0	0
move	0	0.5	0
move	15	0	0
move	0	0.5	0
move	-15	0	0
move	0	0.5	0
move	15	0	0
move	0	0.5	0
move	-15	0	0
move	0	0.5	0
move	15	0	0
move	0	0.5	0
move	-15	0	0
move	0	0.5	0
move	15	0	0
move	0	0.5	0
move	-15	0	0
move	0	0.5	0
move	15	0	0
move	0	0.5	0
move	-15	0	0
move	0	0.5	0
move	15	0	0
move	0	0.5	0
move	-15	0	0
move	0	0.5	0
move	15	0	0
move	0	0.5	0
move	-15	0	0
move	0	0.5	0
move	15	0	0
move	0	0.5	0
move	-15	0	0
move	0	0.5	0
move	15	0	0
move	0	0.5	0
move	-15	0	0
move	0	0.5	0
move	15	0	0

```
move    0       0.5     0
move    -15     0       0
move    0       0.5     0
```

Appendix B: Design of Experiment: Minitab Output

Factorial Regression: Avg FFT versus % C, Length, Speed, Air Pressure, ...

Analysis of Variance

Source	DF	Adj SS	Adj MS	F-Value	P-Value
Model	21	0.015389	0.000733	2.59	0.062
Linear	6	0.007509	0.001252	4.42	0.019
% C	1	0.001383	0.001383	4.88	0.052
Length	1	0.000509	0.000509	1.80	0.210
Speed	1	0.004134	0.004134	14.59	0.003
Air Pressure	1	0.000060	0.000060	0.21	0.655
Nozzle Dia.	1	0.001371	0.001371	4.84	0.052
Standoff Dist.	1	0.000052	0.000052	0.18	0.678
2-Way Interactions	15	0.007880	0.000525	1.85	0.163
% C*Length	1	0.000899	0.000899	3.17	0.105
% C*Speed	1	0.000569	0.000569	2.01	0.187
% C*Air Pressure	1	0.001622	0.001622	5.73	0.038
% C*Nozzle Dia.	1	0.000363	0.000363	1.28	0.284
% C*Standoff Dist.	1	0.000096	0.000096	0.34	0.573
Length*Speed	1	0.000202	0.000202	0.71	0.418
Length*Air Pressure	1	0.001811	0.001811	6.39	0.030
Length*Nozzle Dia.	1	0.000126	0.000126	0.44	0.521
Length*Standoff Dist.	1	0.000022	0.000022	0.08	0.784
Speed*Air Pressure	1	0.000063	0.000063	0.22	0.647
Speed*Nozzle Dia.	1	0.000007	0.000007	0.02	0.879
Speed*Standoff Dist.	1	0.000521	0.000521	1.84	0.205
Air Pressure*Nozzle Dia.	1	0.000727	0.000727	2.57	0.140
Air Pressure*Standoff Dist.	1	0.000722	0.000722	2.55	0.141
Nozzle Dia.*Standoff Dist.	1	0.000129	0.000129	0.46	0.515
Error	10	0.002833	0.000283		
Total	31	0.018223			

Model Summary

S	R-sq	R-sq(adj)	R-sq(pred)
0.0168320	84.45%	51.80%	0.00%

Coded Coefficients

Term	Effect	Coef	SE Coef	T-Value	P-Value
Constant		0.06872	0.00298	23.10	0.000
% C	0.01315	0.00657	0.00298	2.21	0.052
Length	0.00798	0.00399	0.00298	1.34	0.210
Speed	0.02273	0.01137	0.00298	3.82	0.003
Air Pressure	0.00274	0.00137	0.00298	0.46	0.655
Nozzle Dia.	-0.01309	-0.00655	0.00298	-2.20	0.052
Standoff Dist.	0.00255	0.00127	0.00298	0.43	0.678
% C*Length	0.01060	0.00530	0.00298	1.78	0.105
% C*Speed	-0.00844	-0.00422	0.00298	-1.42	0.187
% C*Air Pressure	0.01424	0.00712	0.00298	2.39	0.038

% C*Nozzle Dia.	0.00673	0.00337	0.00298	1.13	0.284
% C*Standoff Dist.	-0.00347	-0.00173	0.00298	-0.58	0.573
Length*Speed	0.00503	0.00252	0.00298	0.85	0.418
Length*Air Pressure	-0.01504	-0.00752	0.00298	-2.53	0.030
Length*Nozzle Dia.	-0.00396	-0.00198	0.00298	-0.67	0.521
Length*Standoff Dist.	-0.00167	-0.00084	0.00298	-0.28	0.784
Speed*Air Pressure	-0.00281	-0.00141	0.00298	-0.47	0.647
Speed*Nozzle Dia.	-0.00093	-0.00047	0.00298	-0.16	0.879
Speed*Standoff Dist.	-0.00807	-0.00404	0.00298	-1.36	0.205
Air Pressure*Nozzle Dia.	0.00953	0.00477	0.00298	1.60	0.140
Air Pressure*Standoff Dist.	0.00950	0.00475	0.00298	1.60	0.141
Nozzle Dia.*Standoff Dist.	0.00402	0.00201	0.00298	0.68	0.515

Term	VIF
Constant	
% C	1.00
Length	1.00
Speed	1.00
Air Pressure	1.00
Nozzle Dia.	1.00
Standoff Dist.	1.00
% C*Length	1.00
% C*Speed	1.00
% C*Air Pressure	1.00
% C*Nozzle Dia.	1.00
% C*Standoff Dist.	1.00
Length*Speed	1.00
Length*Air Pressure	1.00
Length*Nozzle Dia.	1.00
Length*Standoff Dist.	1.00
Speed*Air Pressure	1.00
Speed*Nozzle Dia.	1.00
Speed*Standoff Dist.	1.00
Air Pressure*Nozzle Dia.	1.00
Air Pressure*Standoff Dist.	1.00
Nozzle Dia.*Standoff Dist.	1.00

Regression Equation in Uncoded Units

```
Avg FFT = 0.438 - 0.02391 % C + 0.00455 Length + 0.0635 Speed
          - 0.0163 Air Pressure - 0.288 Nozzle Dia. - 0.1066 Standoff Dist.
          + 0.000042 % C*Length - 0.001125 % C*Speed
          + 0.000949 % C*Air Pressure + 0.00231 % C*Nozzle Dia.
          - 0.000555 % C*Standoff Dist. + 0.000134 Length*Speed
          - 0.000201 Length*Air Pressure - 0.000271 Length*Nozzle Dia.
          - 0.000054 Length*Standoff Dist. - 0.00125 Speed*Air Pressure
          - 0.0021 Speed*Nozzle Dia. - 0.00861 Speed*Standoff Dist.
          + 0.01088 Air Pressure*Nozzle Dia.
          + 0.00507 Air Pressure*Standoff Dist.
          + 0.0110 Nozzle Dia.*Standoff Dist.
```

Alias Structure

Factor	Name
A	% C
B	Length
C	Speed
D	Air Pressure
E	Nozzle Dia.
F	Standoff Dist.

```
Aliases

I + ABCDEF
A + BCDEF
B + ACDEF
C + ABDEF
D + ABCEF
E + ABCDF
F + ABCDE
AB + CDEF
AC + BDEF
AD + BCEF
AE + BCDF
AF + BCDE
BC + ADEF
BD + ACEF
BE + ACDF
BF + ACDE
CD + ABEF
CE + ABDF
CF + ABDE
DE + ABCF
DF + ABCE
EF + ABCD


Fits and Diagnostics for Unusual Observations

Obs  Avg FFT     Fit    Resid  Std Resid
  8   0.1062  0.0824   0.0238       2.53  R
 12   0.0440  0.0679  -0.0238      -2.53  R

R  Large residual
```

Half Normal Effects Plot for Avg FFT

Factorial Regression: Avg FFT versus % C, Length, Speed, Air Pressure, ...

```
Analysis of Variance

Source                   DF    Adj SS    Adj MS  F-Value  P-Value
Model                     7  0.010890  0.001556     5.09    0.001
  Linear                  5  0.007457  0.001491     4.88    0.003
    % C                   1  0.001383  0.001383     4.53    0.044
    Length                1  0.000509  0.000509     1.67    0.209
    Speed                 1  0.004134  0.004134    13.53    0.001
    Air Pressure          1  0.000060  0.000060     0.20    0.662
    Nozzle Dia.           1  0.001371  0.001371     4.49    0.045
  2-Way Interactions      2  0.003433  0.001716     5.62    0.010
    % C*Air Pressure      1  0.001622  0.001622     5.31    0.030
    Length*Air Pressure   1  0.001811  0.001811     5.93    0.023
Error                    24  0.007333  0.000306
Total                    31  0.018223


Model Summary
```

```
        S    R-sq  R-sq(adj)  R-sq(pred)
0.0174796  59.76%     48.02%      28.46%


Coded Coefficients

Term                    Effect      Coef  SE Coef  T-Value  P-Value   VIF
Constant                         0.06872  0.00309    22.24    0.000
% C                    0.01315   0.00657  0.00309     2.13    0.044  1.00
Length                 0.00798   0.00399  0.00309     1.29    0.209  1.00
Speed                  0.02273   0.01137  0.00309     3.68    0.001  1.00
Air Pressure           0.00274   0.00137  0.00309     0.44    0.662  1.00
Nozzle Dia.           -0.01309  -0.00655  0.00309    -2.12    0.045  1.00
% C*Air Pressure       0.01424   0.00712  0.00309     2.30    0.030  1.00
Length*Air Pressure   -0.01504  -0.00752  0.00309    -2.43    0.023  1.00


Regression Equation in Uncoded Units

Avg FFT = -0.090 - 0.02004 % C + 0.00467 Length + 0.01515 Speed
          + 0.00646 Air Pressure - 0.0224 Nozzle Dia.
          + 0.000949 % C*Air Pressure - 0.000201 Length*Air Pressure


Alias Structure

Factor  Name

A       % C
B       Length
C       Speed
D       Air Pressure
E       Nozzle Dia.
F       Standoff Dist.


Aliases

I + ABCDEF
A + BCDEF
B + ACDEF
C + ABDEF
D + ABCEF
E + ABCDF
AD + BCEF
BD + ACEF


Fits and Diagnostics for Unusual Observations

Obs  Avg FFT      Fit     Resid  Std Resid
  8  0.10620  0.07430   0.03190       2.11  R
 26  0.02769  0.06012  -0.03243      -2.14  R

R  Large residual
```